Biomaterials 312 (2025) 122713

Contents lists available at ScienceDirect

Biomaterials

journal homepage: www.elsevier.com/locate/biomaterials

Transcriptomic profiling of human mesenchymal stem cells using a pulsed electromagnetic-wave motion bioreactor system for enhanced osteogenic commitment and therapeutic potentials

Aayushi Randhawa [a,b,1], Keya Ganguly [a,c,1], Sayan Deb Dutta [a], Tejal V. Patil [a,b], Ki-Taek Lim [a,b,c,*]

[a] Department of Biosystems Engineering, Kangwon National University, Chuncheon, 24341, Republic of Korea
[b] Interdisciplinary Program in Smart Agriculture, Kangwon National University, Chuncheon, 24341, Republic of Korea
[c] Institute of Forest Science, Kangwon National University, Chuncheon, 24341, Republic of Korea

ARTICLE INFO

Keywords:
Biophysical stimuli
Pulsed electromagnetic fields
Wave-motion bioreactor
Mesenchymal stem cells
And osteogenesis

ABSTRACT

Traditional bioreactor systems involve the use of three-dimensional (3D) scaffolds or stem cell aggregates, limiting the accessibility to the production of cell-secreted biomolecules. Herein, we present the use a pulse electromagnetic fields (pEMFs)-assisted wave-motion bioreactor system for the dynamic and scalable culture of human bone marrow-derived mesenchymal stem cells (hBMSCs) with enhanced the secretion of various soluble factors with massive therapeutic potential. The present study investigated the influence of dynamic pEMF (D-pEMF) on the kinetic of hBMSCs. A 30-min exposure of pEMF (10V-1Hz, 5.82 G) with 35 oscillations per minute (OPM) rocking speed can induce the proliferation ($1 \times 10^5 \rightarrow 4.5 \times 10^5$) of hBMSCs than static culture. Furthermore, the culture of hBMSCs in osteo-induction media revealed a greater enhancement of osteogenic transcription factors under the D-pEMF condition, suggesting that D-pEMF addition significantly boosted hBMSCs osteogenesis. Additionally, the RNA sequencing data revealed a significant shift in various osteogenic and signaling genes in the D-pEMF group, further suggesting their osteogenic capabilities. In this research, we demonstrated that the combined effect of wave and pEMF stimulation on hBMSCs allows rapid proliferation and induces osteogenic properties in the cells. Moreover, our study revealed that D-pEMF stimuli also induce ROS-scavenging properties in the cultured cells. This study also revealed a bioactive and cost-effective approach that enables the use of cells without using any expensive materials and avoids the possible risks associated with them post-implantation.

1. Introduction

Bone disorders are one of the leading medical conditions requiring innovative therapeutic outcomes. Despite the advent of tissue engineering practices, the most commonly used fracture healing measure includes the use of plasters to restrict bone movement and achieve bone regeneration with or without scaffold implantation. In this scenario, two aspects of the implant play a crucial role in determining the success rate of bone regeneration. One of these is the mechanical property of the implant, while the other involves the distinct bioactivity of the surface chemical property of the implant. Several notable studies have already reported the development of highly strong implants of metal, polymers, and alloys. In contrast, bioactivity has also been reported through the use of biologically derived small molecules, peptides, or functional proteins. Nevertheless, we have not yet accomplished fast bone regeneration. Alternatively, the use of cell-based therapies that may expedite bone regeneration over a short period, ranging from days to weeks after scaffold implantation, has great potential as a faster method for bone regeneration [1,2]. In this context, bone healing can be facilitated using stem cell therapy and tissue engineering techniques that incorporate biomaterials and preconditioned stem cells.

Mesenchymal stem cells (MSCs) have received the greatest research attention in bone regeneration [3–6]. Thousands of patients experience bone-related complications yearly, such as osteosarcoma, osteoarthritis,

* Corresponding author. Department of Biosystems Engineering, Kangwon National University, Chuncheon, 24341, Republic of Korea.
E-mail address: ktlim@kangwon.ac.kr (K.-T. Lim).
[1] These authors have contributed equally to the manuscript.

https://doi.org/10.1016/j.biomaterials.2024.122713
Received 13 February 2024; Received in revised form 22 July 2024; Accepted 25 July 2024
Available online 26 July 2024

and fractures, among which each patient requires a cell range of 10^5 to 10^{10} cells for therapy [7]. Clinical studies showed that stem cell transplantation is an outstanding technique to combat organ damage. However, the practical application of stem cell-based therapeutics is hindered due to the limitations in the large-scale expansion culture of MSCs [8–10]. Therefore, it is imperative to identify more effective stem cell culture methodologies to meet the criteria for large-scale expansion and osteogenic preconditioning of stem cells [11].

To address this need, recent advancements have focused on exposing cells to externally applied physical stimuli, such as shear stress and magnetic, electric, and electromagnetic fields (EMFs), which induce mechanotransduction-mediated stem cell proliferation and differentiation [12–16]. In the physiological *in vivo* environment, fluid shear, and matrix strain play a significant role in influencing bone hemostasis by stimulating mechanosensory functions [17]. For instance, osteocytes, the predominant cells found in bone, function as primary mechanosensors and regulators of bone metabolism. Through mechanotransduction, they govern bone development and resorption by secreting various signaling molecules that influence the activity of osteoblasts and osteoclasts [18].

Numerous bioreactor systems have been developed in conjunction with physical stimulation techniques to elicit specific responses in stem cells, representing a significant advancement for translational applications in bone regeneration and therapeutics. These sophisticated bioreactors stimulate stem cell proliferation, differentiation, and functional maturation by mechanical and physical stimulation [19]. For instance, electrical stimulation in bioreactors enhances stem cell osteogenic development, resulting in bone-like structures with improved bone matrix production [20]. Pulsed electromagnetic fields (pEMFs) similarly increase the expression of osteogenic markers and enhance mineralization [21]. Additionally, the mechano-sensitivity of MSCs cultured in a pulsatile-pressure bioreactor system has been shown to promote osteogenic differentiation on soft matrices [22]. Moreover, external mechanical forces such as compression, tension, and fluid shear are often used to promote stem cell growth and osteogenic differentiation [23].

Despite such advancements, we are yet to achieve a bioreactor stimulation system that can enhance stem cell proliferation and differentiation for advanced therapeutic applications. We hypothesized that while each type of stimulation individually has been shown to enhance stem cell proliferation and therapeutic applications, their combined application could offer several unique advantages.

Considering the abovementioned conditions, in the present study, we devised a custom-built rocking bioreactor system for expanding human bone-marrow-derived mesenchymal stem cells (hBMSCs) under combined effects of wave motion and pEMFs to monitor proliferation and osteogenic behavior for cell-based therapeutics. Scheme 1 represents the stem cell-based therapeutic bioreactor setup, and the study design is aimed at hBMSCs' regulation and therapeutic outcomes. To the best of our knowledge, this investigation has not been previously reported. The primary goal of our study was to develop a cost-effective scaffold-free stimuli-responsive expansion of the hBMSCs, triggering the secretion of biologically active molecules to encourage rapid bone regeneration in a matter of days and weeks. We chose wave motion stimulation to mimic the natural mechanical forces that cells experience *in vivo,* while pEMFs can activate various cellular signaling pathways to achieve cell proliferation. Given the current constraints in bone regeneration, including

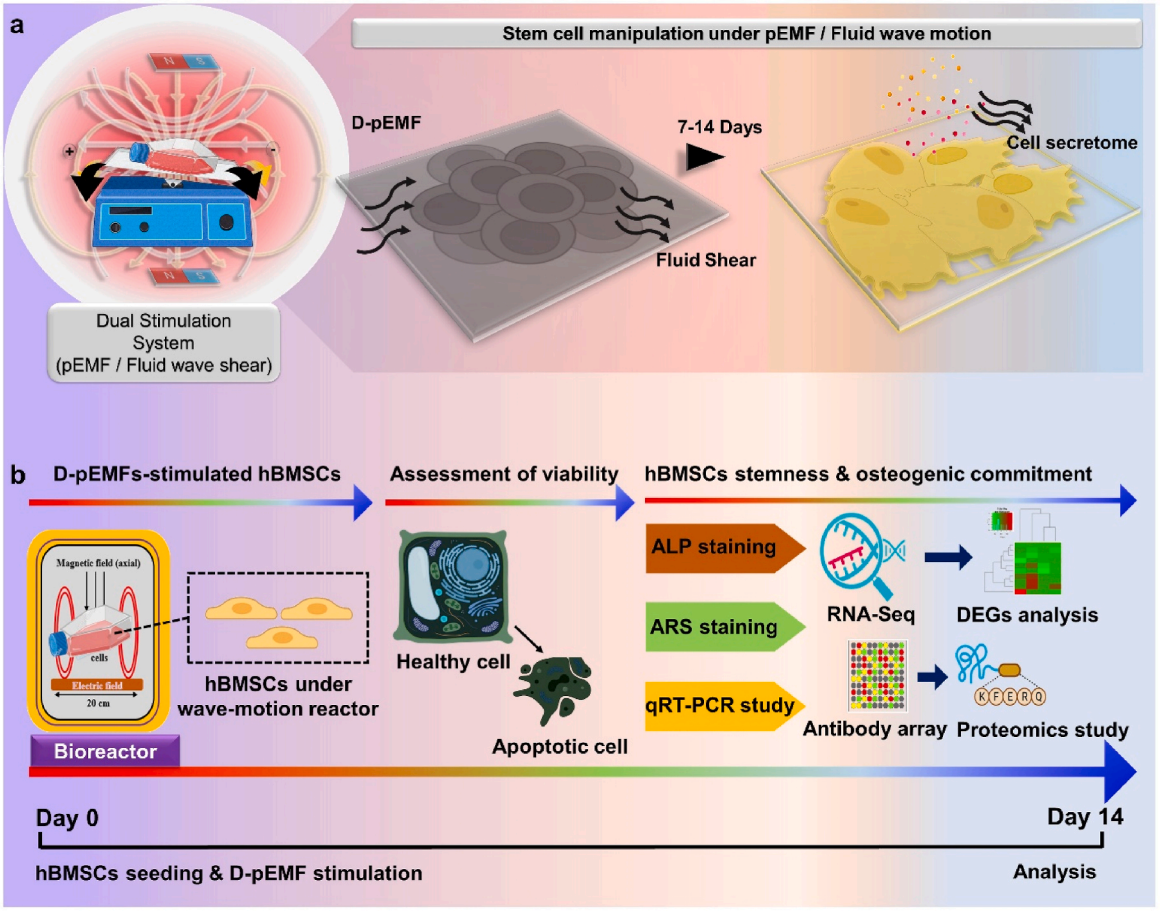

Scheme 1. A schematic depiction of stem cell-based therapeutic bioreactor stimulation setup. **(a)** The hypothetical representation of the effect of dynamic-pulsed electromagnetic field (D-pEMF) stimuli in promoting osteogenic commitment. **(b)** The overall design of the study over a period of 14 days considering stimulation and the assessment of human mesenchymal stem cell proliferation and osteogenic commitment.

low proliferation rate, poor bioactivity, and lengthy healing processes, we envision that our study will significantly advance pEMF-stimuli-based therapeutics by promoting rapid stem cell proliferation, enhanced cell secretion, rapid osteogenic differentiation for stem cell-based therapeutic applications. Furthermore, it can help in the development of pEMF-based wearable devices, facilitating more efficient bone repair in the future.

2. Material and methods

2.1. Materials

Human bone marrow-derived mesenchymal stem cells (hBMSCs, PromoCell C-12974) supplemented with Fetal bovine serum (FBS) (Welgene Inc., Republic of Korea), Dulbecco Modified Eagle Medium (DMEM), 1 % antibiotics (P/S), and phosphate buffer saline (PBS) were purchased from Welgene, Republic of Korea. The Live-Dead staining kit, osteo-inductive media, RNAzol, F-actin probe, osteo-inductive media, ALP, ARS detection kit, and 4,6-diamino-2-phenylindole dihydrochloride (DAPI) were obtained from Sigma-Aldrich, USA. The PrimerScript™ reverse transcriptase kit, and SYBR green qRT-PCR master mix was bought from TaKaRa Bioscience, Japan. The primary and secondary antibodies against ALP, Runx2, Ki67, ERK ½, and MEK were purchased from Santa Cruz Biotechnology, USA. The gene primers were acquired from BIONEER Inc., Daejeon, Republic of Korea. Human growth factor C1 and cytokine antibody C5 array were bought from Raybiotech, USA. A custom-designed wave-motion bioreactor with an externally controlled pEMF system was acquired from Lee-Chun Electronics Ltd., South Korea. *In vitro* glucose and lactate assay kits were obtained from DoGenBio, Republic of Korea.

2.2. Design of wave-motion bioreactor and optimization

In this study, we utilized a custom-designed bioreactor system consisting of multiple sensors such as pH, humidity, CO_2, glucose, and lactate sensors connected via a peristaltic pump to displace the suspension. The bioreactor is connected via an pEMF generator, which produces the pEMF through the EMF coils. The experi

mental conditions were optimized by considering different parameters such as rocking speed, voltage, and frequencies to evaluate the effective state of treatment with the control group. Table 1 represents an overview of the four experimental groups selected for this study with the stimuli duration of 30 min for 7 and 14 days.

2.3. In vitro study

2.3.1. hBMSCs culture

The hBMSCs maintained in DMEM with 10 % fetal bovine serum, 1 % P/S comprising (10000 Units mL^{-1}) penicillin, (10000 g mL^{-1}) streptomycin in a humidified environment of 5 % CO_2 at a temperature range of 37 °C (Steri-Cycle 370 Incubator; Thermo-Fisher Scientific, USA). The passage-3 or passage-4 of (1.0×10^5 hBMSCs/100 μL DMEM media) were seeded in a 25 mm^3 flask. After two days of culturing the cells in DMEM media, the cell culture medium changed to osteogenic media. Upon reaching 70–80 % confluency, the cells in the culture flask were used for the treatment under a wave-motion bioreactor.

Table 1
A list of various treatment groups was used in this study.

Sl. No.	Group	*p*-EMFs stimulation	Rocking motion (35 rpm)	Time of stimulation
1	S	No	No	No
2	D	No	Yes	30 min/day
3	S-pEMF	Yes	No	30 min/day
4	D-pEMF	Yes	Yes	30 min/day

S: Static; D: Dynamic; pEMF: Pulse electromagnetic fields.

2.3.2. Cell viability assay

For the cell viability assessment, the 1.0×10^5 hBMSCs were cultured into different 96-well plates and maintained in a CO_2 incubator. After culturing cells with treatment conditions for a desired duration (days 1, 7, and 14), the viability was assessed utilizing the WST-8 assay kit protocol. Briefly, the sample media was incubated with 10 μL of WST-8 dye for 1–4 h at 37 °C in the dark. By examining the absorbance at 450 nm, the generated formazan was quantified. The results are represented as average OD ± standard deviations; each experiment was carried out in triplicate.

2.3.3. Live-dead assessment

The cell population of 1.0×10^5 cells was suspended in culture media and cultured on a 4-well plate in a humidified environment with 5 % CO_2 at 37 °C under different experiment conditions. The cell survivability following various treatments was then analyzed utilizing live and dead fluorescence photography after 7 and 14 days of treatment. For the live/dead assay, the cells were washed with PBS and incubated with 10 μL of ethidium bromide and acridine orange dye with a ratio of 1:1 for 5–10 min at 37 °C. Afterward, the cells were photographed using an inverted fluorescence microscope (DMi8 Series, Leica, Germany) with appropriate filters.

2.3.4. Characterization and morphological assessment of hBMSCs

The stemness of the hBMSCs under all experimental conditions was evaluated by the fluorescence-activated cell sorting (FACS) technique. For this, the 1.5×10^6 cells were fixed with the 3.7–4% paraformaldehyde for 10 min, followed by suspending in 1X PBS containing 1 % BSA for half an hour to block the un-specific antibody-linking sites. After that, the blocked cells were treated with particular primary antibodies, including CD34, CD90, CD13, and CD146, for 1 h at 4 °C, followed by 1 h treatment with fluorescently tagged secondary antibodies. All the antibodies used were bought from BD Biosciences in San Jose, California, United States. The FACS caliber flow cytometer from BD Biosciences, Immuno-cytometry system, San Jose, United States, was then used to calculate the CD34, CD90, CD13, and CD146 positive cell percentages. Cell Quest Pro program was then used to examine the results. Additionally, to validate the results of FACS for maintaining stemness, we further performed the gene expression of stemness markers in treatment groups using qRT-PCR. In brief, the cells 10×10^4 in the culture media were cultured according to the experiment conditions for 7 and 14 days. The total RNA was extracted by harvesting the treated cells using RNAzol reagent under the manufacturer's recommendations. A spectrophotometer was used to evaluate the concentration and purity of the extracted RNA. The qRT-PCR against the *NANOG* gene maker was performed utilizing a CFX96 Maestro Real-Time system, Bio-Rad (USA). For morphological evaluation, the 1×10^5 hBMSCs/100 μL media were cultured on the surface of the cover glass for 7 and 14 days. The cells were maintained and imaged regularly in the microscope to check the proliferation rate and morphology. After completing the treatment duration, the cells on the cover glass were fixed using 3.7 % PFA for 15 min and washed twice with PBS. Next, the cells were dehydrated using different gradients of ethanol. Finally, cells were dried using ethanol and hexamethyldisilazane (HDMS) (50:50 ratio). A scanning electron microscope (UR-SEM, Hitachi-S4800, California, USA) was employed to study the effect of D-pEMF on cell morphology.

2.3.5. Analysis of cellular metabolites

Cell metabolism-related components, such as glucose and lactate, were monitored using a built-in glucose/lactate sensor in various culture conditions. We have checked the level of glucose and lactate form (from) the used (collected) media via glucose/lactate assay kits (DoGenBio, Republic of Korea), respectively.

2.3.6. Cell cycle pattern analysis

The cell cycle evaluation was conducted using PI stain. In short, after treatment, the cells were washed and trypsinized. The cells were then washed using PBS and centrifugated to obtain the pellet. The pellet was then fixed overnight using 70 % iced ethanol at 4 °C. After that, the fixed cells were incubated at 37 °C with 300 μL RNase A-PI solution. A flow cytometer (FACS Calibur, BD Bioscience, San Jose, USA) and BD CellQuest Pro software (BD Bioscience, USA) were utilized to interpret the results. The cell percentage at Sub-G0/G1, G0/G1, S, and G2/M phases were computed and compared with each experimental group.

2.3.7. Analysis of reactive oxygen species (ROS)

The H_2O_2-prompted oxidative damage in various treatment groups was assessed using qRT-PCR, dichlorodihydrofluorescein diacetate (DCF-DA) dye, and the GSH activity was evaluated. For qRT-PCR, the 10 × 10^5 cells/100 μL media were cultured and treated under different treatment conditions. Next, the total RNA was collected using the RNAzol method in accordance with the manufacturer's instructions. The cDNA was then generated using reverse transcriptase enzyme and SYBR Green Master mix from 2 μg of RNA. The gene expression of ROS scavenging genes (*GPX, TXNR1, NOX4, CAT, SOD2)* and a senescence-regulating gene (*Bcl2)* was measured using Bio-Rad Real-Time PCR (CFX96TM Maestro Real-Time System, Bio-Rad, USA). The primer sequences of all the forward and reverse primers used in ROS and senescence markers gene expression are presented in Table S1.

Next, the 1 × 10^5 cells were cultured in 24 well plates in DMEM media. Subsequently, the cells without H_2O_2 were considered as negative control, and cells treated with 200 μM H_2O_2 for 30 min were taken as positive control and were incubated at 37 °C in a CO_2 incubator. Following the treatment, the cells were then incubated with 20 μM DCF-DA dye for 30 min. Next, the cells were washed twice with PBS. The fluorescence intensity of DCF-DA was measured with a fluorescence microscope (ex/em = 485/538). The corresponding intensities of DCF-DA were determined for the quantitative study of the generation of intracellular ROS by using ImageJ software (ImageJ v1.8, NIH Lab., Bethesda, MD, USA, https://imagej.nih.gov/). Radioimmunoprecipitation assay (RIPA) buffer was used to extract the total protein for GSH activity. Subsequently, I mL of 0.5 × 10^{-3} M 5,5-dithiobis-(2-nitrobenzoic acid) (DNTB) was mixed with 0.2 mL of protein lysate and allowed to stand for 5 min at room temperature. The overall GSH activity was then measured at 405 nm spectrophotometrically. Data from three replicated studies (n = 3) presented as mean ± SD.

2.4. Osteogenic induction and mineralization study

For osteogenic differentiation, the 10 × 10^5 cells/100 μL were cultured in osteogenic induction media containing DMEM supplemented with 50 μg/mL L-ascorbic acid, 10 mM β-glycerophosphate, and 100 nM dexamethasone, respectively. In order to assess the effects of treatment conditions on the cultured cells, culture media samples were collected from each group every 2 days for a duration of 14 days. The Alizarin Red-S (ARS) staining was performed according to the manufacturer's instructions, the cells were washed with PBS twice, fixed with 70 % ice-cold ethanol, and stained by 40 mM alizarin Red-S stain (pH 4.2) for 1 min, and the nodule formation was photographed using a digital camera and the optical microscope. To evaluate the amount of mineralization, the cells were destained using 10 % cetylpyridinium chloride (CPC) for 30 min, and the absorbance of the resulting solution was measured spectrophotometrically at 562 nm. Furthermore, the cells for alkaline phosphatase staining were performed using an alkaline phosphatase detection kit (Sigma-Aldrich, USA) following the manufacturer's protocols. Images were taken using an inverted light microscope (Carl Zeiss, Germany).

Moreover, on days 7 and 14, the collected supernatant was centrifuged to eliminate the cell debris and inspected to quantify the alkaline phosphatase (ALP), an osteoblast marker enzyme and tartrate-resistant acid phosphatase kits (TRAP), an osteoclast marker enzyme. As per the manufacturer's guidelines, the harvested supernatants were treated with ALP and TRAP kits (Takara, Japan). Briefly, the collected supernatants were incubated with 50 μL the *para*-nitrophenyl phosphate substrate for 30 min, and the absorbance was taken at 405 nm. A standard curve of absorbance versus *p*-nitrophenol concentration was plotted and used to evaluate the concentration of nitrophenol in/∼M/mL. The current investigation presents all values as absorbances determined at 405 nm. The harvested cell culture media was incubated with 10 % acetic acid at 85 °C for 10 min for calcium content quantification.

2.5. Cytoskeletal morphology study

The organization of cell cytoskeletal F-actin was evaluated after 7 and 14 days of treatment by using an inverted fluorescence microscope (DMi8 Series, Leica, Germany) with appropriate filters. Briefly, the 1 × 10^5 cells/100 μL media were cultured according to the experimental groups. Following 7 and 14 days of treatment, the cell fixation and permeabilization were done using 3.7–4% paraformaldehyde (PFA, Sigma, USA) and 0.1 % Triton-X 100. Then, 1 % BSA was used to block the cells for 1 h and washed with PBS. Next, the cells were stained with F-actin Red and counterstained with DAPI to visualize the F-actin and nucleus. The stained cells were then rinsed, mounted with mounting solution, and covered using a glass coverslip. The fluorescence photographs were taken using a super high-resolution CLSM (Carl Zeiss, Germany), and images were analyzed with ZEN software (v1.8, Carl Zeiss, Germany).

2.6. RNA extraction and qRT-PCR analysis

The gene expression of osteogenic markers in treatment groups was assessed using qRT-PCR. In brief, the cells 10 × 10^5 cells/100 μL culture media were cultured according to the experiment conditions for 7 and 14 days. The total RNA was extracted by harvesting the treated cells using RNAzol reagent under the manufacturer's recommendations. A spectrophotometer was used to evaluate the concentration and purity of the extracted RNA. The synthesis of cDNA was performed using 2 μg of RNA by employing reverse transcriptase enzyme and SYBR Green master mix. The qRT-PCR against osteogenic gene markers (*Runx2, ALP, OCT4, NFκ-β, Col1, OSX, OPN, PIEZO*) and signaling pathway gene markers (*Smad1, TGF-β, RANKL,* and *AKT)* were conducted employing a CFX96 Maestro Real-Time system, Bio-Rad (USA). The reaction protocols involved 43 denaturation cycles for 15 s at 95 °C and 60 s amplification at 60 °C. All the experiments were conducted in triplicate and normalized to the GAPDH housekeeping gene, as described in our prior study [24,25]. The sequences of all the forward and reverse primers used in osteogenic and signaling pathway-specific gene-markers expression are presented in Table S2.

2.7. Transcriptome analysis

The transcriptomic evaluation was conducted to investigate the differentially expressed genes (DEGs) in several treatment groups. Following 7 days of expansion culture, the total RNA was collected using RNAzol reagent. The typical RNA library was created using the extracted RNA. A next-generation RNA sequencer (Nova-Seq 6000, PE100 bp, CA, USA) was used to carry out the QuantiSeq 3′ mRNA-Seq utilizing the human UCSC and genome hg19 reference genome database. The raw data were normalized to log2 (mean of normalized data in every group), and Student's *t*-test was used for statistical evaluations.

2.8. Immunocytochemical staining

The immunocytochemical staining was performed to study the expression of osteogenic and signaling markers. For this, the hBMSCs of 1.0 × 10^4 cells/100 μL were cultured and treated for 7 and 14 days.

Following the treatment, the cells were washed and fixed with 3.7 % PFA for 15 min at room temperature. Next, the permeabilization was done using 0.1 % Triton X-100 for 10 min. Next, the cells were rinsed and blocked by 1 % BSA, and using 250 μL of mouse monoclonal antibodies against Runx2, ALP, MEK1, and ERK$^{1/2}$. A 20 μL of 1 mg/mL DAPI solution (1–2 min) was used to counterstain the nucleus in the dark. The fluorescence photographs were captured using a microscope at a magnification of 20X.

2.9. Proteomics study

The proteomic changes of the hBMSCs with or without D-pEMF treatment were evaluated using protein antibody arrays. The treated groups' cytokine and growth factor array were performed in accordance with the manufacturer's protocol using Raybiotech Human Antibody array kit (Raybiotech, USA), namely human cytokine antibody array C5 and human growth factor array C1. The densitometry results were acquired using the ImageJ software (v1.8, NIH, Bethesda, USA). The obtained data was normalized to positive control spots, and the interaction between secreted proteins was evaluated using STRING v12.0 (www.string-db.org) software. The *k*-means clustering was performed with a 0.999 confidence level with a PPI enrichment score less than <0.05.

2.10. Statistical analysis

The statistical analysis used Origin Pro v9.0 (Origin Labs, USA). The significant variation among the control and treatment groups was determined using the One-way Analysis of Variance (ANOVA) test.

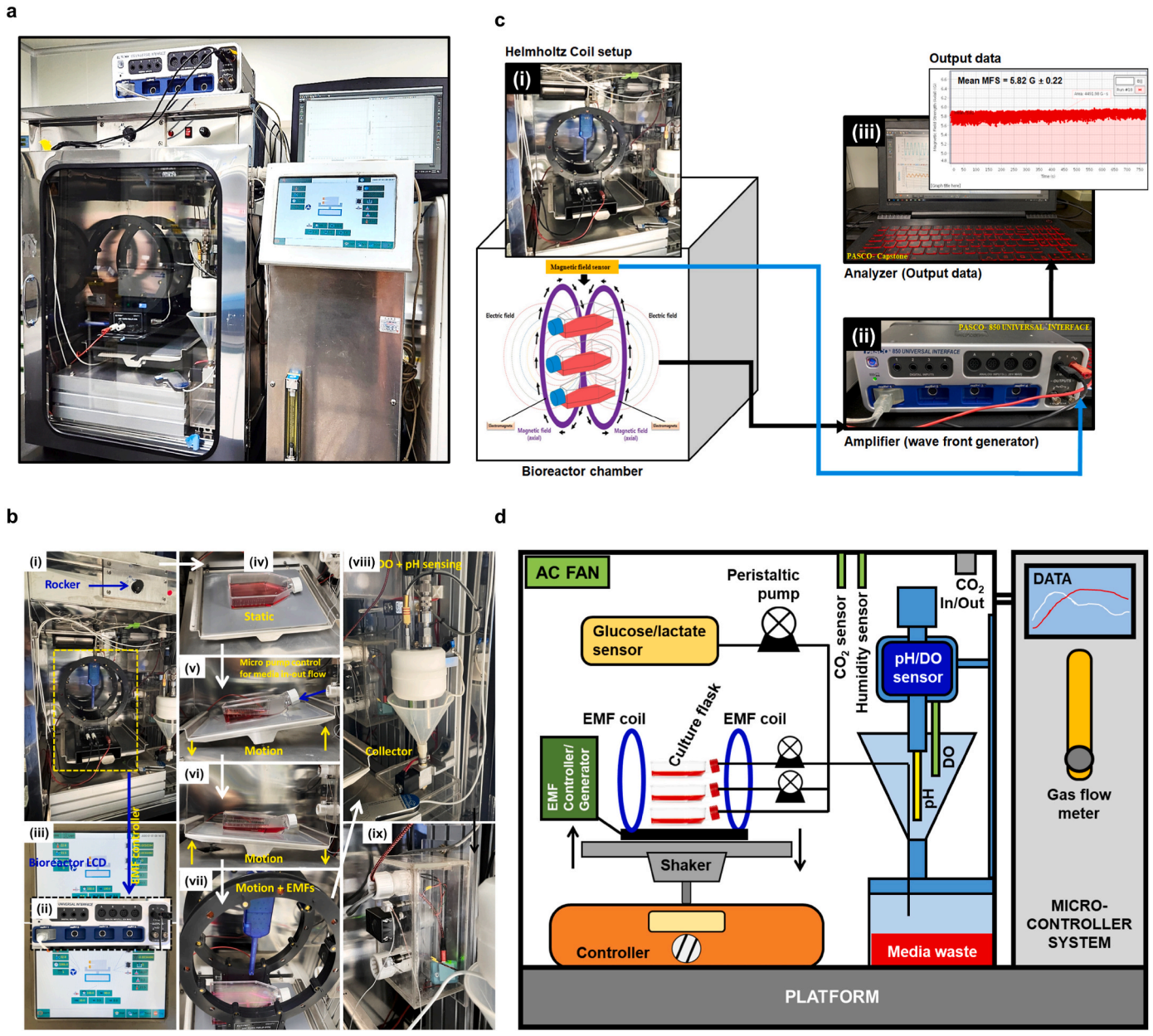

Fig. 1. Bioreactor set-up and function. **(a)** A digital photograph of the wave-motion bioreactor. **(b)** (i) The rocking knob for the seesaw movement of the cells. (ii) A PASCO 850 universal interface setup for pEMF generation. (iii) An LCD screen for detecting the real-time condition of the experiment. (iv-vii) The four experiment groups showing S, D, S-pEMF/D-pEMF conditions. (viii-ix) DO/pH and glucose sensors connected to the reactor system to detect the alteration during experiments. **(c)** Schematics of the pEMF stimulation system. (i) The coils were placed exactly in the center of the wave-motion rocker with an MF sensor. (ii) The external amplifier connected the coils (PASCO-850 Universal Interface, USA). (iii) The amplifier can be controlled through PASCO Capstone software using a portable laptop. The MF sensor data shows that the coils can generate a pEMF of about 5.82 ± 0.22 G. **(d)** The overall schematic illustration of the bioreactor setup.

Statistical significance was considered at $*p < 0.05$, $**p < 0.01$, and $***p < 0.001$. The Student's *t*-test was used to assess the RNA-Seq data.

3. Results

3.1. Bioreactor design and performance

A digital photograph of the custom-built pEMF-wave motion bioreactor system is shown in Fig. 1a. The bioreactor chamber consisted of an incubator with an integrated rocking platform and two additional Helmholtz coils to generate the desired wave flow (seesaw motion) and pEMF simultaneously.

The rocker platform induced an oscillatory wave motion of the culture media onto adhered hBMSCs. This wave motion of the cells can be controlled with the help of the rocker controller unit, which allows for the adjustment of different oscillation per minute (OPM) settings (Fig. 1b (i)). Additionally, a real-time temperature controller and CO_2 gas flow system were used to replicate the environment of a native biological oxygen demand (BOD) within the bioreactor. These conditions were regulated via a real-time monitoring touch screen TFT LCD, which could be controlled from outside the reactor (Fig. 1b (ii, iii)). Fig. 1b (iv-vii) depicts the various experimental conditions (S, D, S-pEMF, D-pEMF) that can be created inside the bioreactor system by controlling the rocking speed of the rocker and the EMF. An automated media flow control with a real-time dissolved O_2 and pH (DO/pH) sensing device (500 × 300 mm) was integrated to monitor the change in media pH during the cell expansion culture (Fig. 1b (viii, ix).

A PASCO 850 universal interface (California, USA) was utilized to generate pEMF stimulation. The device can produce several waveforms, such as triangular, sinusoidal, ramp, and square (with DC offset), having a frequency ranging from 0.001 to 100 kHz. The setup is made of a waveform function producer (15 W) with a power amplifier (PASCO Power Amplifier-II, CI-6552A, up to ±10 V peak at 1 A), the two-axis magnetic field sensor (MF sensor; PS-2162, PASCO Scientific, range ±1000 G, max. sample rate 1000 Hz) linked to the amplifier, and the two Helmholtz coils placed 20 cm apart. Both Helmholtz coils were made with copper wires (0.64 mm diameter, 500 turns) with an outer and inner radius of 11.37 and 10.06 cm, respectively (Fig. 1c). Each coil was covered with a polycarbonate-based plastic layer to avoid external damage. The signals were shifted to the coils using an amplifier. The coils producing the pEMF and the MF sensor were placed inside the 5 % CO_2 incubator. At the tip of the sensor's probe, the MF sensors have two separate Hall effect components oriented perpendicularly to each other. For this study, we have positioned the MF sensor vertically among the two coils to estimate the axial magnetic field inside the bioreactor. The experimental setup of the current study is schematically depicted in Fig. 1d and Video S1-S3.

3.2. Effects of D-pEMF on hBMSCs cellular activity

3.2.1. Stimulation optimization and biocompatibility assessment

We optimized the stimulation condition for effective hBMSCs expansion and therapeutic secretion. The pEMF stimulation of various time durations has been reported to promote proliferation in previous studies [26,27]. To determine the optimal duration for effective cellular results, we optimized our experimental design by considering various parameters, including rocking conditions and exposure time. The hBMSCs were exposed to rocking conditions of 0, 15, 25, 35, 45, and 55 OPM for 30 min/24h. An increased percentage of viable cells was noted in the cells exposed to 25, 35, and 45 OPM w.r.t. the control group (0 OPM) post 24 h of treatment. In contrast, no significant difference was observed in the cell viability between 25 and 35 OPM (Fig. S1a). Hence, hBMSCs exposed to 25–45 OPM were further evaluated for their cell viability under altered stimulation period (15, 30, and 60 min), as shown in Fig. S1b. A significant increase in the cell viability was observed in the hBMSCs exposed to 35 OPM for 30 min w.r.t. other counterparts. Therefore, 35 OPM/30 min was considered for our experiments.

Further, the hBMSCs viability was monitored under different magnetic field frequencies (0, 1, 10, and 15 Hz) under two different voltages, 10V and 15V. Stem cells cultured under pEMFs operated at over 10 V are shown to create high-gradient magnetic forces that significantly affect cell functions, shape, and spatial organization. Despite the low diamagnetic susceptibilities of cellular components, high-gradient magnetic fields are shown to induce substantial changes by exerting forces proportional to the field gradient on the cells and cellular components. This interaction can enhance cellular responses, making pEMF exposure effective for stem cell proliferation and differentiation [28]. Our experimental data showed no significant differences in the cell viabilities (Fig. S1c); however, the hBMSCs cultured under 1Hz-10V showed significantly increased cell proliferation ability (Fig. 2a).

Following optimal conditions, a 10V-1Hz pEMF stimulation, generating an average magnetic field of 5.82 ± 0.22 G, is judiciously chosen for the bioreactor culture of hBMSCs. Each culture flask or plate received a 10V-1Hz pEMF stimulation for 30 min/day for 7–14 days. The hBMSCs were differentiated in an osteogenic induction medium for the desired period using the same condition.

Next, to comprehend the effects of all four treatment conditions (S, D, S-pEMF, and D-pEMF) on hBMSCs survivability, the cell viability evaluation was performed at various time intervals (1, 7, and 14 days). We observed a significant rise in the cell viability of hBMSCs exposed to D-pEMF following 1 and 7 days of treatment (Fig. 2b). Furthermore, we saw a progressive improvement in cell viability after a 14-day treatment period. Subsequently, the live-dead staining experiment was conducted using the acquired cell viability data. Our investigation revealed that the hBMSCs exhibited excellent biocompatibility, as no observable cell death was seen after 7 and 14 days of growth in all experimental settings (Fig. 2c). The experimental groups were characterized by a prominent presence of green fluorescence, which indicated the population of alive cells. The vitality of the cultivated hBMSCs remained over ~80 % on both the 7th and 14th days, suggesting that none of the treatment conditions exhibited toxicity towards the cells. Our observation suggests that the viability of the cells remained intact in all of the treatment groups.

3.2.2. Stemness properties of the hBMSCs under stimulation

A FACS analysis was conducted to confirm the effects of stimulation on maintaining the stemness of hBMSCs. Following treatment of 7 and 14 days, we observed a consistent expression of the key stemness markers in hBMSCs across all the experimental groups, including CD 13, CD 146, CD 34, and CD 90. A major population of cells in each group expressed over ~95 % (day 7) and ~80 % (day 14) of CD13 and ~80 % of CD146 in each group (Fig. 2c). The percentage of stemness markers CD13 and CD90 on days 7 and 14 further revealed an expression percentage of over 70 % in all treatment conditions on days 7 and 14 (Figure S2 (a, b)). Moreover, the level of *NANOG* expression was assessed to provide additional confirmation of the stemness of hBMSCs (Fig. 2e). The gene expression data revealed a significant upregulation of *NANOG*, with a fold increase of about 9.4-fold at day 7 and approximately 6.7-fold under D-pEMF stimuli, compared to the control group ($***p < 0.001$). The expression values of *NANOG* across different treatment groups are given in Table S3.

The stemness properties were further investigated through morphological changes and photographed at different durations (1, 3, and 7 days). As shown in Fig. 2f and Fig. S4, the hBMSCs experienced a spindle-like morphology, and the division trend rapidly expanded. On day 1, cells exhibited a large population of spindle-shaped cells, while the cells under the D-pEMF stimuli showed a transition in shape from spindle-to-stellate or star-shaped cells from day 3 (Fig. S4), as observed through the optical microscopic images. Additionally, the SEM images revealed an increased population of spindle-shaped cells in the S group with a smaller number of cells obtaining stellate shape, while a star-like

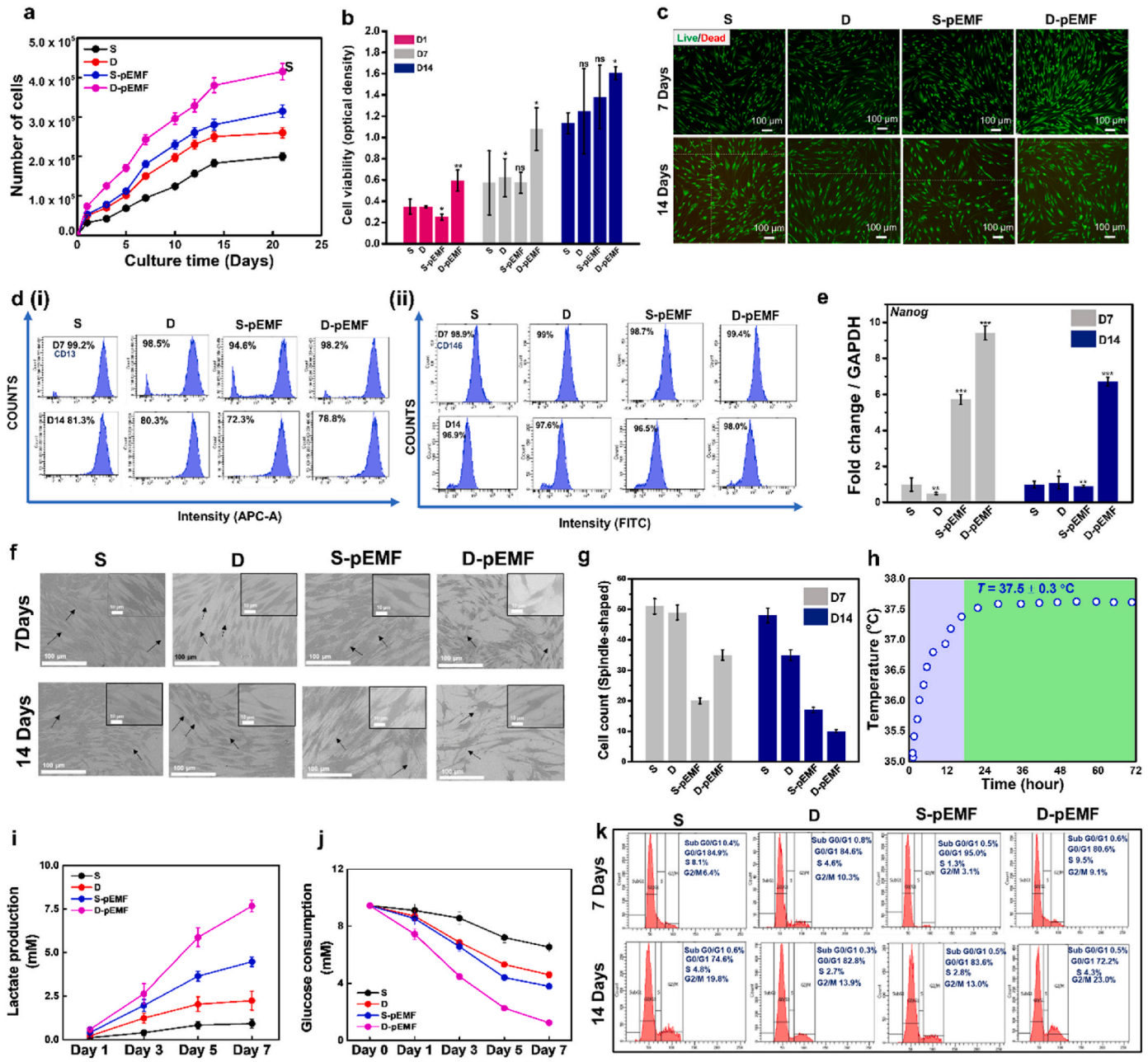

Fig. 2. The biocompatibility assessment and characterization of hBMSCs upon D-pEMF. **(a)** The cell proliferation rate of hBMSCs cultured under various treatment conditions at a different time interval. **(b)** Colorimetric WST-8 assay of the cells cultured in different treatment conditions on Day 1, 7, and 14. **(c)** Representative live/dead assay of the hBMSCs in various treatment conditions. **(d)** Fluorescent-activated cell sorting (FACS) analysis of the hBMSCs showing the expression of CD13 and CD146 surface makers of the cells culture under different experimental conditions. **(e)** Gene expression of stemness marker *NANOG* is used to check the stemness markers' expression in treatment groups. **(f)** SEM images of cells cultured in various treatment conditions to study the morphological changes upon treatment. **(g)** The total cell count of the different shaped cells was analyzed through SEM images. **(h)** The relative temperature changes of the bioreactor as a function of time. **(i)** Glucose consumption, and **(j)** Lactate production of hMSCs in various treatment groups at indicated time points. **(k)** Cell cycle analysis of the cells cultured under various stimuli to study the effects of cell proliferation in treatment conditions. All the images were taken on day 7 (grey bar) and 14 (blue bar) following the treatment. (For interpretation of the references to colour in this figure legend, the reader is referred to the Web version of this article.)

shape change in the morphology of S-pEMF and D-EMF group cells indicating the effects of pEMF conditions in attaining osteoblast differentiation (Fig. 2f and g).

3.2.3. *D-pEMF enhances hBMSCs metabolism*

As a standard procedure in all subsequent experiments, the conditioned medium was obtained from the cultured cells following the various treatment parameters. The resulting metabolites in the conditioned medium were compared to elucidate the potential of pEMF on the cells. The temperature range in the bioreactor was maintained at 37.2 ± 2 °C throughout the study Fig. 2h. Following 7 days of the culture, cell metabolic activity was assessed by evaluating the respective groups' glucose and lactate production in the culture media. Upon 7 days of treatment, the D-pEMF group produced 1.2 mM glucose, which was relatively lower than the S group 6.54 mM (Fig. 2i). In contrast, the lactate amount was evaluated as 7.67 mM in the D-pEMF group, and the S group contained 0.92 mM. Altogether, cells cultured in the D-pEMF group generated the highest lactate in the culture media concerning the

control and other treatment groups. Glucose production follows a reverse trend, indicating the activated cell metabolism by producing lactate as a by-product of glycolysis during the metabolic activity. These results indicate that the D-pEMF culture of hBMSCs plays an important role in regulating cell metabolism and effectively metabolizing glucose into lactate compared to the S culture group (Fig. 2j).

3.2.4. *D-pEMF induces rapid hBMSCs division*

The progression of the cell cycle in hBMSCs cultured under different treatment conditions was evaluated. The D and D-pEMF stimulation was observed to promote a comparable percentage of cells in the active G2/M phase, indicating their higher proliferative states w.r.t. S and S-EMF groups. While considering the cell growing phase, we observed that 84.9 % of cells in the S group are in the G0/G1 phase, with a 10 % reduction rate at day 14. No significant effect was observed in the cells cultured in D conditions post 14 days' treatment condition. The cells in S-pEMF exhibited a higher percentage of G0/G1 population of 95.0 % at day 7 compared to other groups, with a reduction of~11.4 % following 14 days of culture. The cells cultured under the D-pEMF group exhibited 80.6 % of the cell population in the G0/G1 phase, which is less when compared with other groups at day 7. On day 14, the cells cultured under the D-pEMF group exhibited the highest population of cells in the G2/M phase with a percentage of 23 % compared to other treatment groups Fig. 2k. These results indicate that D-pEMF stimuli induce higher cell division and proliferation.

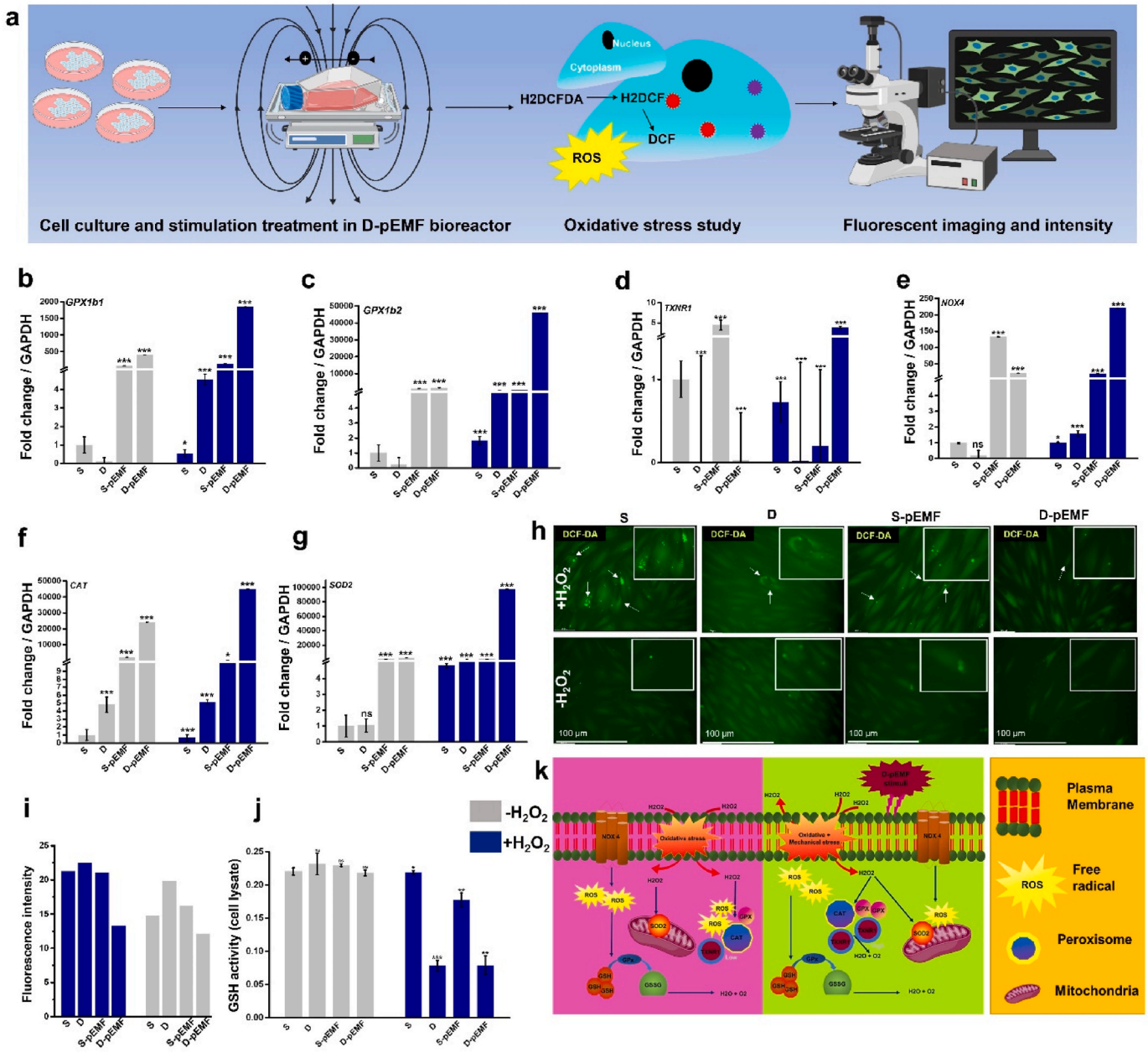

Fig. 3. In vitro ROS assessment of the different treatment conditions. **(a)** A schematic depiction of the 30-min treatment conditions. **(b–g)** Gene expression analysis of ROS-scavenging genes, including *GPX*, *TXNR1*, *NOX4*, *CAT*, and *SOD2* using qRT-PCR post 7 days (grey bar) and 14 days (blue bar) of treatment. **(h–i)** ROS scavenging assessment; green fluorescent images of DCF-DA in hBMSCs after 20 min of incubation with ($\pm$ H_2O_2) following 7 days of treatment with their corresponding intensity profiles. **(j)** Quantitative analysis of total GSH activity under different treatment conditions. **(k)** A hypothetical representation of the mechanism involving the stimuli-assisted ROS scavenging activity. (For interpretation of the references to colour in this figure legend, the reader is referred to the Web version of this article.)

3.2.5. Activation of cell ROS scavenging properties

Despite the role of pEMF stimulations in enhancing cell proliferation and bone regeneration [29,30], several epidemiological research studies have suggested that pEMF stimulation might increase the incidence of cancers. For instance, the pEMF stimulation of 50-50 Hz is reported to cause apoptosis, chromosomal instability, and activation of cell cycle checkpoints [29]. Therefore, to investigate the impact of pEMF stimulation on hBMSCs, we further examined the impacts of D-pEMF in inducing oxidative damage, as illustrated in Fig. 3a.

To confirm the mechanism of D-pEMF stimulation in regulating ROS production, we examined the gene expression analysis of different ROS scavenging and ROS-generating genes. The major categories of antioxidants, namely glutathione peroxidase (*GPX1b1, GPX1b2*), selenoprotein thioredoxin reductase 1(*TXNR1),* NADPH oxidase 4 (*NOX4),* catalase (*CAT*), and superoxide dismutase 2 (*SOD 2*) genes were selected for gene expression study that was up and downregulated upon different treatment conditions (Fig. 3b–g). The gene expression analysis revealed that the control group ($-/+H_2O_2$) shows a slight or basal level change in gene expression of *SOD2, CAT, TXNR1, NOX4, GPX1a, GPX1b1,* and *GPX1b2.* On the contrary, the D-pEMF treatment group exhibited an increased level of *GPX1b1, GPX1b2, TXNR1, NOX4, CAT,* and *SOD2* in both ($-/+H_2O_2$) conditions when compared with other treatment groups. The gene expression results of all the treatment groups are given in Table S4. Our findings suggested that the cells treated under the D-pEMF group have the potential to induce ROS-scavenging properties in the cells.

Next, we employed H_2O_2-triggered oxidative stress by H_2DCF-DA, as shown in Fig. 3h. In the negative control configuration (without H_2O_2 and stimuli), a low level of ROS generation was noted, indicating the physiological production of ROS. On the other hand, in the positive groups (with H_2O_2), including (S, D, S-pEMF, and D-pEMF), a significant ROS production was observed in the S group (with H_2O_2), while the other groups exhibited lower or basal levels of ROS production. The fluorescence intensities confirmed a decreased level of ROS production in the D-pEMF group (Fig. 3i).

Furthermore, the GSH activity as depicted in Fig. 3j showed a reduced level of glutathione in the H_2O_2 treated groups, indicating its possible involvement in the reduction of H_2O_2, leading to its conversion into its oxidized form glutathione disulfide (GSSG) and water [31].

As oxidative stress in associated with cellular senescence [32], we further evaluated the expression of senescence marker *Bcl2*. Among all the experimental groups, the D-pEMF showed a reduced expression (~0.8-fold) compared to the control group, further strengthening the anti-oxidative effects of D-pEMF in cellular senescence (Fig. S3). The gene expression results of all the treatment groups are given in Table S5. The results indicated that the exposure of D-pEMF to the cells activates the anti-oxidative properties [33]. Hence, these outcomes verified that the hBMSCs exhibited higher proliferative, stemness, and ROS scavenging characteristics in D-pEMF culture conditions. The involvement of GSH and other oxidative enzymes is illustrated in Fig. 3k.

3.3. D-pEMF promotes osteogenic differentiation of the hBMSCs

3.3.1. Mineralization increment and osteoclast activity reduction

Acknowledging the fact that the pEMF stimulation accelerates the osteogenic potential of hBMSCs [34], we investigated the effects of the D-pEMF conditions in the osteogenic development of the hBMSCs, the mineralization capabilities of the hBMSCs cultured in the groups as mentioned earlier was first utilized for Alizarin Red Staining (ARS). Fig. 4a depicts the ARS-stained photographs of the hBMSCs in different groups at 7 and 14 days. The S (control) groups depict no mineralized nodule development following a culture duration of 7 days, and a slight nodule formation was observed at 14 days of culture, which indicates a delayed onset of nodule generation in the absence of stimuli. In contrast, an increasing trend of mineralized nodule formation has been seen in the other groups. The group with D-pEMF conditions exhibits a dense distribution of the nodule formation, demonstrating the superior mineralization potential induced by the D-pEMF condition.

Furthermore, the quantitative comparison of the mineral content in the treatment groups was quantified following the destaining method (Fig. 4b). The cells treated with D-pEMF conditions showed enhanced mineralization at 7 days and 14 days compared to the control group. Moreover, the calcium content quantification from different groups' collected cell culture media showed an increased calcium content level in cells treated with D-pEMF conditions (Fig. 4c). Next, to confirm the osteogenic capability of the D-pEMF stimuli, the ALP activity was assessed, and an increased stained area in the D-pEMF group was revealed (Fig. 4d). An increase in ALP activity by ~250 μg/500 μL was observed in the hBMSCs under D-pEMF stimuli w.r.t. the S group (Fig. 4e).

Owing to the osteogenic potential of D-pEMF conditions, the acid phosphatase (ACP) quantification assay was performed to evaluate the impact of D-pEMF's role in osteoclast genesis. The results of ACP quantification revealed an increase in ACP secretion by ~39 μg/mL in the S group compared to the D-pEMF group upon 7 days of treatment. In contrast, an enhancement of ~69 μg/mL in the S group was observed following 14 days of treatment (Fig. S5). These results indicate that the D-pEMF conditions can be used as a potential candidate for suppressing osteoclast activity.

3.3.2. Cell morphology and osteogenic protein expression

The actin cytoskeleton arrangements on the treated cells were evaluated using an inverted fluorescence microscope (DMi8 Series, Leica, Germany) with appropriate filters, and the results are given in Fig. 4f. We observed an organized distribution of actin in the D-pEMF group with higher microfilaments. In contrast, the S group revealed poor fluorescence intensity and a less organized cytoskeleton. Increased cytoskeletal organization has been associated with enhanced mechanotransduction-mediated hBMSC differentiation [35,36]. Hence, we assume that the actin distribution in the hBMSCs under D-pEMF might play a crucial role in determining the hBMSCs' proliferation and differentiation ability.

Interestingly, ALP and Runx2 expressions during the treatment were tracked for up to 7 and 14 days (Fig. 4g and h). The immunostaining results showed an expression and improved distribution in all the treatment groups. Together, these findings suggest the role of D-pEMF in accelerating osteogenic protein expression and inducing morphogenesis by altering the cytoskeleton arrangements upon treatment.

3.3.3. Expression of osteoblast-specific gene markers

To verify the lineage determination, we subsequently carried out the qRT-PCR. We utilized against osteogenic gene markers (*Runx2, ALP, OCT4, NFκ-β, Col1, OSX, OPN*), and signaling pathway gene markers (*PIEZO-1, Smad1, TGF-β, RANKL,* and *AKT)* were conducted employing a CFX96 Maestro Real-Time system, Bio-Rad (USA), as described in our prior study [24,25]. We analyzed the gene expression of osteogenesis markers in the cells with control and treatment conditions. The D-pEMF treatment significantly influenced the expression of all the osteogenic markers. The four genes were selected based on the early and late osteogenesis markers. The increased *ALP* and *RUNX2* expression levels signaled the beginning of hBMSCs osteogenic differentiation under D-pEMF conditions. At the same time, the late osteogenic markers *OPN* were found to increase significantly in the D-pEMF group. Cell culture in the D-pEMF group for 7 and 14 days displayed an enhanced mRNA level of *RUNX2 ALP*, *OCT4*, *NFκ-β*, *Col1*, *OSX, OPN*, and *PIEZO 1*, remarkably higher than the S group (Fig. 4i–p). The gene expression results of the osteogenic gene markers represented in (Table S6) confirm the expression of the osteogenic protein marker under D-pEMF conditions. The obtained gene expression data indicates the positive effects of D-pEMF exposure in promoting osteogenesis, which is consistent with the protein expression of *ALP* and *Runx2*.

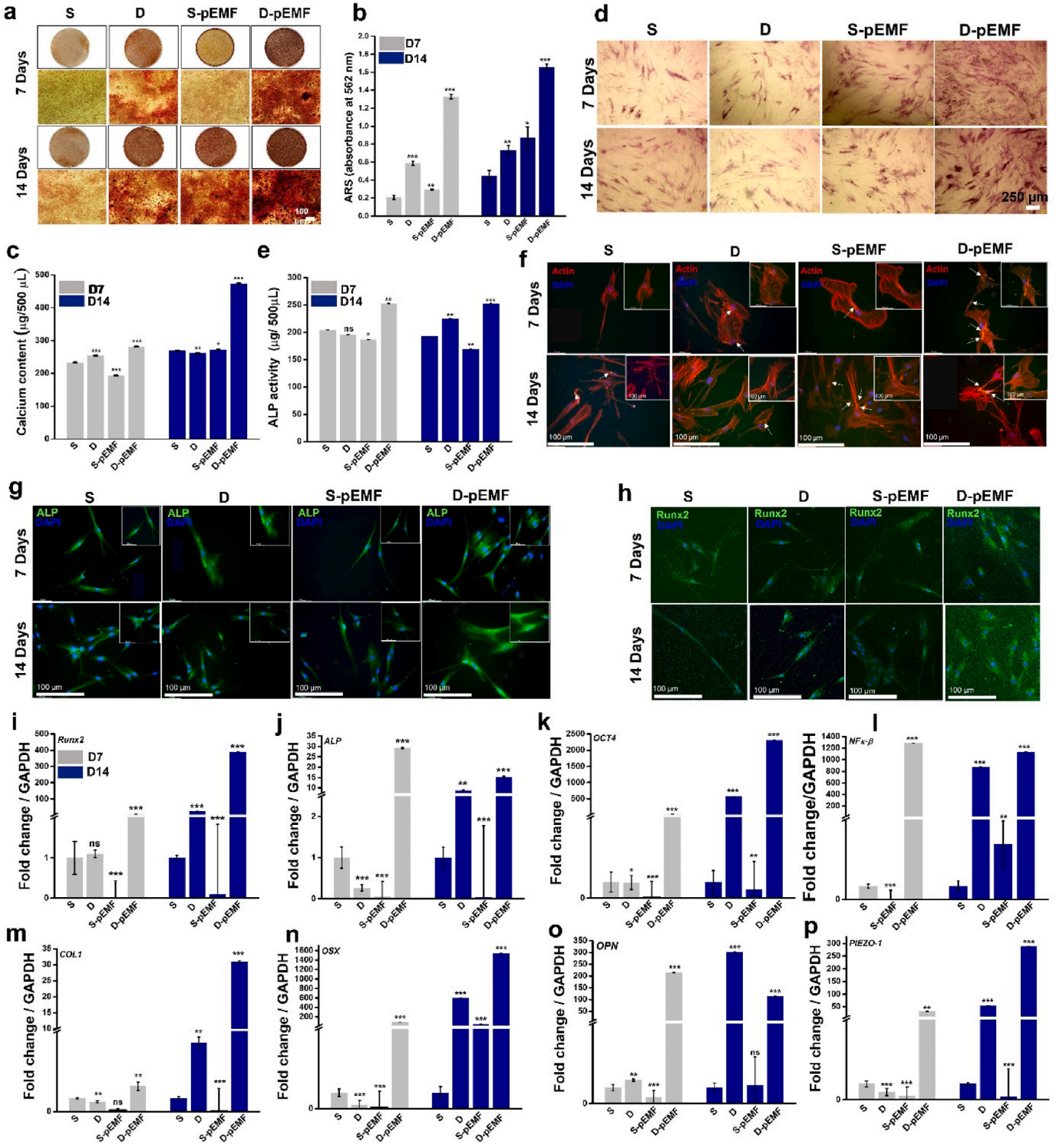

Fig. 4. Osteogenic differentiation potential of hBMSCs under D-pEMF treatment. Mineralization study of the hBMSCs showing **(a)** Digital and microscopic photographs of ARS-stained cells under different treatments at days 7 and 14. Scale bar: 100 µm **(b)** Quantification of the mineralization in ARS-stained cells under various treatment conditions. **(c)** Quantitative analysis of the calcium content secretion in cell supernatant upon 7and 14days treatment. **(d)** ALP-stained cells at different time intervals. Scale bar 250 µm. **(e)** Quantitative analysis of the ALP activity from the cell supernatant following treatment. **(f)** Fluorescent images of the actin cytoskeleton (red) and nucleus (blue) after 7 and 14 days of culture. Scale bar: 100 µm. **(g–h)** protein expression of osteogenic protein ALP and Runx2 in different treatment groups at days 7 and 14. Scale bar: 100 µm. **(i–p)** Real-time PCR evaluation of the genes associated with the osteogenic proliferation, such as *Runx2*, *ALP*, *OCT4*, *NFκ-B*, *Col1*, *OSX*, *OPN*, and *PIEZO1*. (For interpretation of the references to colour in this figure legend, the reader is referred to the Web version of this article.)

3.4. Transcriptomic analysis revealed the involvement of multiple pathways in hBMSCs under D-pEMF exposure

The RNA sequencing data demonstrated that approximately 805 genes out of 25737 were differentially expressed, showing a significant change during osteogenic differentiation of hBMSCs in various culture conditions (Figs. S6a and b). Depending upon the differentially expressed genes (DEG), the most upregulated and downregulated genes were chosen for the data investigation. The DEGs were further subjected to unbiased hierarchical clustering and *k*-means clustering and represented as heatmap in Fig. 5a–b. We inspected the RNA sequencing of osteogenic differentiation-related DEGs in hBMSCs. According to the clustering data, it was evident that the D-pEMF group exhibited distinct transcriptomic changes compared to the other groups. Among the various clusters, Cluster-C of the D-pEMF group exhibited higher expression of osteoblast differentiation-related DEGs than other treatment groups. The *k*-means enrichment score (with a *p*-value <0.05) of the clustered groups with upregulated pathways is presented in Fig. 5c.

Interestingly, in Cluster-C, the highly upregulated terms identified were cell differentiation (Enrichment score: 7e-15) and ossification (Enrichment score: 5e-51), indicating the positive role of D-pEMFs on osteogenesis. Similarly, the enrichment in ossification (Enrichment score: 3e-83) in cluster-A, osteoblast differentiation (Enrichment score: 8e-44) and skeletal system development (Enrichment score: 2e-21), skeletal system morphogenesis (Enrichment score: 2e-14) in cluster-B, connective tissue development (Enrichment score: 6e-20) and cartilage development (Enrichment score: 5e-20) in cluster-D also signifies the endochondral tissue regeneration potential of hBMSCs in D-pEMF

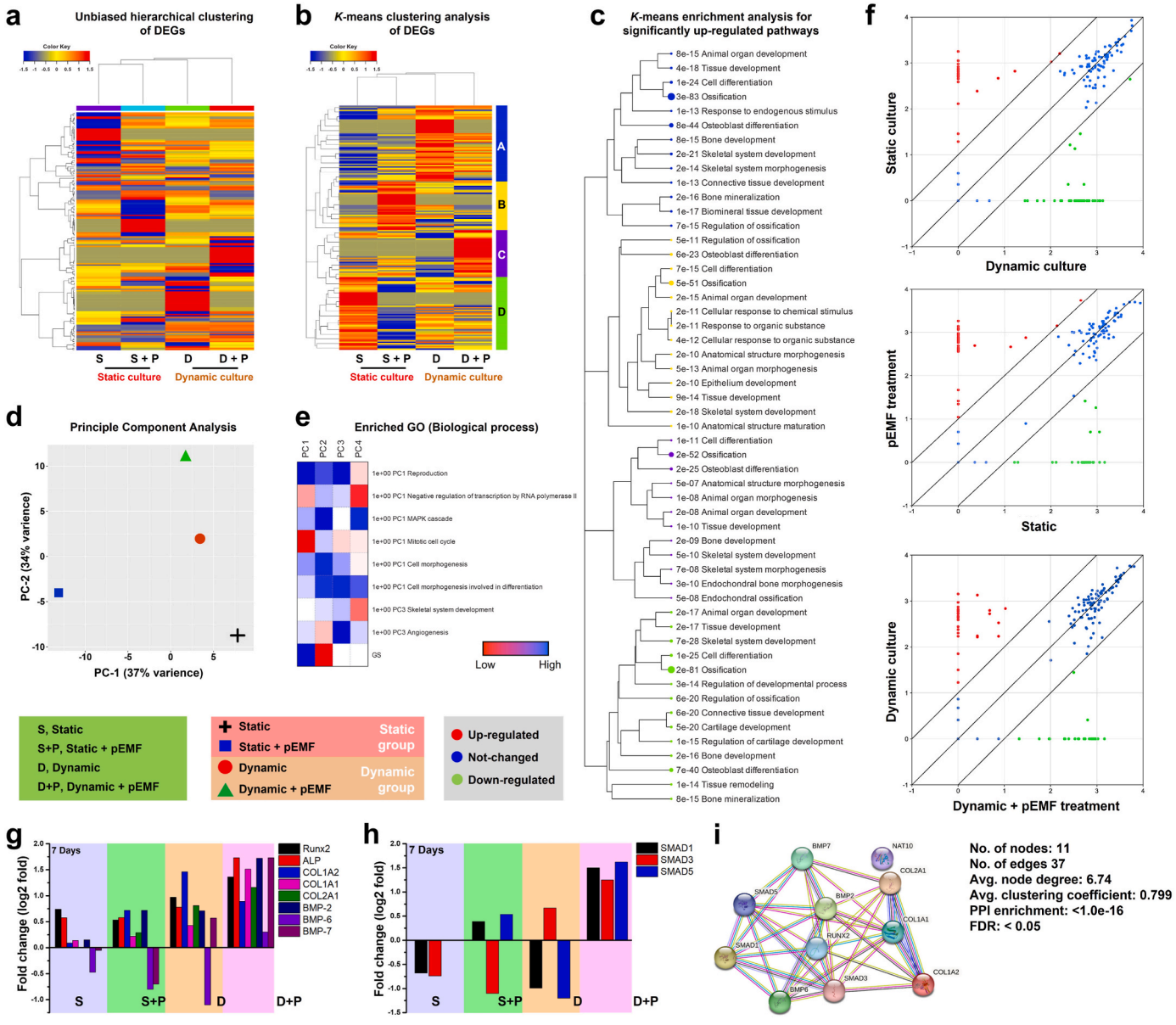

Fig. 5. Transcriptomic changes of the hBMSCs under various culture conditions. **(a)** Unbiased hierarchical clustering of differentially expressed genes (DEGs) associated with osteoblast differentiation after 7 days of culture. **(b)** K-means clustering of the DEGs associated with osteogenesis. Four clusters were represented with a mean k-value of 0.749. **(c)** Representative PPI enrichment score of various pathways related to osteoblast differentiation. **(d)** Principle component analysis (PCA) of the various treatment groups. **(e)** Representative heatmap showing the gene ontology (GO) enrichment associated with a biological process in PCA. **(f)** Representative scatter plots of DEGs in various treatment groups show up- or down-regulated genes. **(g)** Fold change (Log2 fold) of various osteogenic genes analyzed through RNA-Seq. **(h)** Fold change (Log2 fold) of various SMAD genes analyzed through RNA-Seq in various culture conditions. **(i)** STRING interaction map of the osteogenic transcription factors.

groups [37–39]. The principal component analysis of the treatment groups was carried out to evaluate the gene-gene separation. The analysis revealed that the DEG coupled with osteogenic differentiation was not clustered, indicating more than one osteoblastic event participation during osteogenesis (Fig. 5d). To determine the cell differentiation of hBMSCs upon various treatments, we examined the biological process through gene ontology (GO) enrichment analysis. In the D-pEMF group, the GO terms such as MAPK cascade, cell morphogenesis involved in differentiation, and skeletal system development were significantly upregulated, as shown in Fig. 5e. The scatter plot of the expressed genes reveals the drastic variation in expression arrangement during different culture conditions**.** Importantly, PCNA, a nuclear transcription factor, is highly expressed in the D-pEMF-treated groups (27.89-fold), compared to S (2.29-fold), D (2.85-fold), and S-pEMF groups (2.9-fold), respectively. Moreover, EIF2B4 expression was upregulated during the D-pEMF culture (2.29-fold) of hBMSCs, suggesting that D-pEMF culture exhibited more cell proliferative function and differentiation potential than static culture.

Fig. 5f shows the scatter plot of differentially expressed genes (DEGs) in various conditions when compared between static/dynamic (S/D), dynamic/dynamic pEMF (D/D-pEMF), static/dynamic pEMF (S/D-pEMF), and dynamic/dynamic pEMF (D/D-pEMF), respectively. Compared to S culture, in D-pEMF culture, 71 genes were found to be upregulated, and 38 genes were down-regulated during osteogenesis. Notably, no significant genes were up- or down-regulated when compared between dynamic vs. dynamic pEMF groups, meaning that pEMF-mediated dynamic culture shows more differentially expressed genes (DEGs) than other treatment groups (Fig. 5f). Notably, 155 genes were down-regulated, and 426 were upregulated when compared between different treatment conditions, indicating that the D-pEMF stimulation of hBMSCs was more metabolically active than the static culture.

Next, we analyzed the principle DEGs associated with osteogenesis from cluster C. We found an enhanced expression of Runx2 (~1.3 fold) and ALP (~1.7 fold) in the D-pEMF group than the S group, which follows the qRT-PCR data (Fig. 5g). The DEGs were also found to be involved in the SMAD signaling pathways, a key signaling pathway influencing osteogenesis. The transcriptome of the D-pEMF group showed an increased expression of SMAD1 (~1.5 fold), SMAD3 (~1.25 fold), and SMAD5 (~1.62 fold), as indicated in Fig. 5h. It is well-reported that the electromagnetic field improves the osteogenic capability of the hBMSCs via alteration of SMAD signaling [40]. The Runx2 interacts with SMADs via direct linking to a transcriptional stimulator complex. Runx2 employs Regulatory SMADS (R-SMADS) to form a complex to start osteogenesis signaling [41]. The STRING protein-protein interaction map of the identified transcription factors with their corresponding linkage is represented in Fig. 5i.

Based on the results of transcriptomic data revealing the involvement of signaling pathways such as *Smad1, TGF-β, and MAPK*, we further validated the participation of these pathways by performing real-time qPCR analysis for gene expression at 7 and 14 days (Fig. 6). The results showed an increased level of *Smad1* (~10-fold) in the D-pEMF group on day 7, which was then reduced to half (~5-fold) on day 14 (Fig. 6a). We also observed a drastic enhancement in the *SMAD1* expression in the S-pEMF group (~1726.4-fold) at day 14. We also confirm the expression of *TGF-β,* which was found to be higher in the D-pEMF group at day 7 (~25.6-fold) and day 14 (~1.6-fold) compared to the S group (Fig. 6b). Additionally, the enhancement in gene expression analysis of mechanotransduction genes involved in osteogenesis, such as *RANKL* and *AKT,* showed an increased expression upon treatment (Fig. 6c and d), confirming their role in osteogenic commitment [22, 42–44]. Additionally, the immunocytochemistry results showed the protein expression of ERK1/2 and MEK1 (Fig. 6e and f). The gene expression results of the studied signaling pathways across all the treatment groups are given in Table S7. Together, the gene expression results proved the involvement of the signaling pathway, as revealed by the transcriptomic analysis.

To analyze the osteogenic differentiation of hBMSC under the D-pEMF culture, we further carried out the gene set enrichment analysis (GSEA). The circos diagram displaying the inter-relationship among the genes involved in various biological processes is depicted in Fig. 7a. According to the (GSEA) score of the biological processes in Fig. 7d, it is clear that more than 160 genes are associated with ossification, whereas more than 80 genes are linked to osteoblast differentiation. Fig. 7b shows the circos plot of the DEGs involved in cellular components; out of the DEGs, approximately 20 genes comprise the collagen-containing extracellular matrix, cell-substrate junction, focal adhesion, endoplasmic reticulum lumen, transcription regulation complex, and approximately 5 genes associated with the banded collagen fibril, and fibrillar collagen trimer Fig. 7e. The molecular function of the DEGs was further assessed to determine the function performed by the multiple

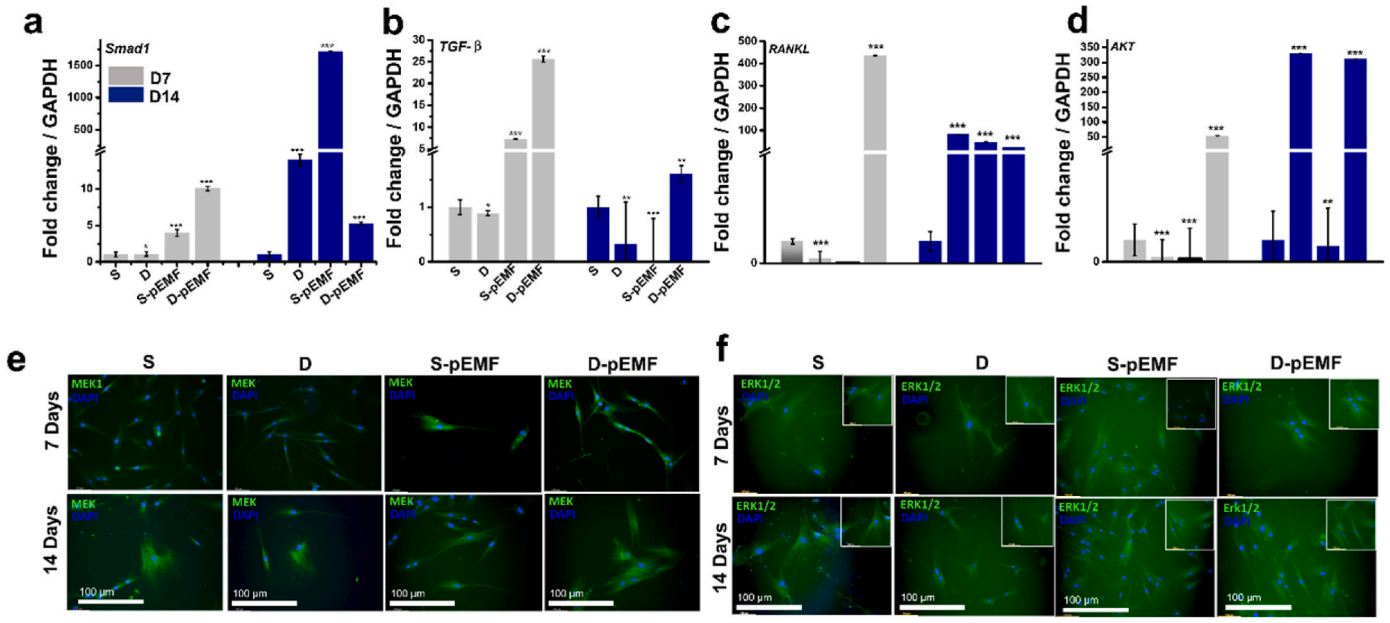

Fig. 6. Evaluation of signaling pathways involved in transcriptomic analysis. **(a–d)** Gene expression study of various signaling markers such as Smad1, TGF-β, RANKL, and AKT. **(e–f)** Protein expression of signaling markers MEK1 and ERK1/2 in treatment groups following 7 and 14 days of treatment. Scale bar: 100 μm.

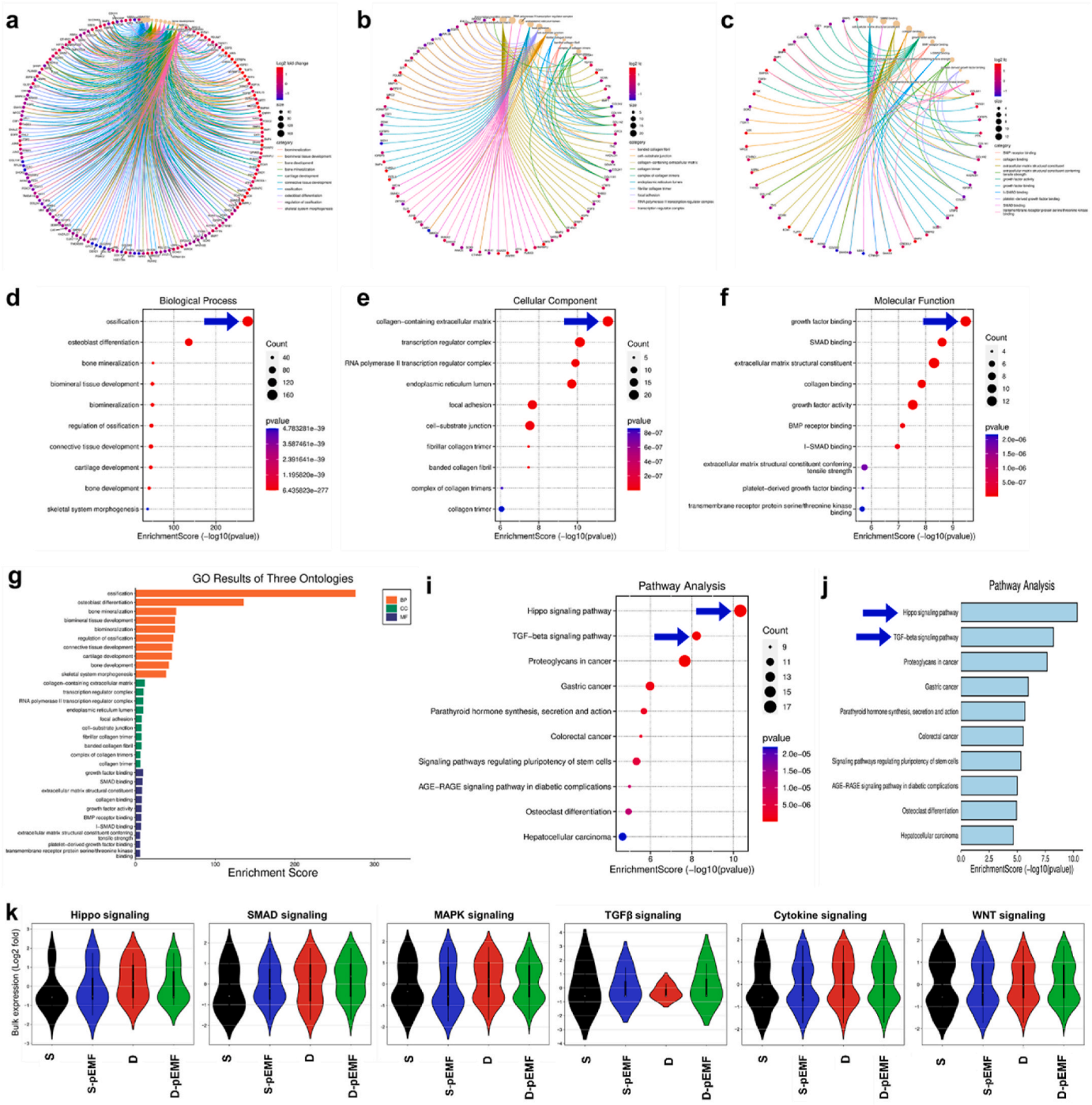

Fig. 7. Gene set enrichment analysis (GSEA) of the hBMSCs undergoing osteogenic differentiation during D-pEMF culture. Circos diagram of the hBMSCs in D-pEMF group showing the interaction of various genes associated with **(a)** biological process (BP), **(b)** cellular component (CC), and **(c)** molecular function (MF). **(d–f)** Representative GSEA enrichment score in BP, CC, and MF of hBMSCs in D-pEMF group with corresponding enrichment bubbles. **(g)** The GO results of the three ontologies. **(h, i)** GSEA pathway enrichment during D-pEMF culture of hBMSCs. (j) Bulk expression (Log2 fold) of various genes associated with Hippo, SMAD, MAPK, TGF-β, cytokine, and Wnt signaling pathways during D-pEMF culture.

genes by plotting the circos diagram Fig. 7c, the genes contributing the growth factor binding, extracellular matrix structural constituent, growth factor activity comprised of 12 gene counts, while more than 10 genes mainly, SMAD1, SMAD3, BMP-2, BMP-1, involved in SMAD binding which further involved in SMAD-dependent BMP/SMAD signaling pathway. In Smad-dependent signaling, the BMP ligand binds to its corresponding receptor and leads to the phosphorylation of Receptor-Smad (R-Smad, including Smad1/5/8) to the Smad4 and forms a complex. This complex then translocates into the nucleus and regulates the osteogenic differentiation [45]. The three ontologies, biological process, cellular component, and molecular functions, are summarized in Fig. 7g, indicating the majority of gene counts involved in ossification and osteoblast differentiation. A pathway analysis study was performed on the cells cultured in D-pEMF conditions to determine the signaling pathways associated with the DEGs. Mainly, two signaling pathways, the Hippo signaling pathway and TGF-β signaling, influence the osteogenic differentiation in our study (Fig. 7h–i). The overall summary of the signaling pathways impacted by our study is given as a bulk expression

of genes (Log2 fold) in Fig. 7j; the D-pEMF treatment group showed a comparative upregulation of genes associated with Hippo, Smad, MAPK, TGF-β, Cytokine, and WNT signaling pathways than the other groups.

3.5. Secretome analysis of hBMSCs exposed to D-pEMF stimuli

The proteomic changes of the hBMSCs under S and D-pEMF conditions are evaluated using the antibody array employing secretory proteins from 7 days of treatment, and the results are shown in Figs. S7a–b. Two antibody arrays were performed: growth factor array and cytokine array. As depicted in Fig. S7a, there was no significant alteration in the expression of secreted growth factors in both S and D-pEMF conditions. However, the cytokine array exhibited changes in the secretion pattern of hBMSCs in S and D-pEMF groups (Fig. S7b). For instance, the expression of BNDF (1.2 fold), TIMP-1 (1.55 fold), Angiogenin (Ang, 1.12 fold), and IGFBP-2 (1.42 fold) were found sufficiently higher in the D-pEMF group than the S group. BNDF is a neurotropic factor that induces osteoblast migration and is involved in fracture healing [46]. TIMP1, a member of metalloprotease-1 inhibitor, has been shown to inhibit osteogenic differentiation and affect the cancellous bone mineralization via the Wnt/β-catenin signaling pathway [47]. Similarly, Ang and IGFBP-2 are primarily involved in vascularized bone healing via paracrine signaling with hBMSCs [48,49]. Therefore, our results suggest that the D-pEMF stimulation of hBMSCs induced osteogenic inductor and inhibitory proteins after 7 days of culture in a wave-motion bioreactor. The expression profile of major secretory growth factors and cytokines is shown in Fig. 8a.

We further studied the protein-protein interaction using STRING software to understand the role of various secretory proteins in hBMSCs stemness and osteogenic differentiation. The result is displayed in Fig. 8b. The *k*-means clustering (clustering co-efficient: 0.771, PPI enrichment score: 3.83e-08) revealed the presence of three main clusters among the interacted proteins, of which cluster-1 includes 5 proteins (MMP2, TIMP1, IL6, CCL2, and CXCL8), cluster-2 consists of 7 proteins (IGF1, IGF1R, IGFBP2, IGFBP4, IGFBP5, and IGFBP6), and cluster-3 includes 5 proteins (VEGFA, PGF, FLT4, NRP1, and KDR), respectively.

The VEGF and their receptors are considered pro-lymphogenic factors that promote vascularization. Hao et al. reported that 30 ± 3 Hz 5 mT exposure of pEMF elevated the VEGF secretion and phosphorylation of endothelial nitric-oxide synthase in an ischemic muscle by abolishing the effect of phosphatidylinositol-3-kinase (PI3K) which concluded that the vascularization-induced potential of EMF and activation of PI3K/AKT/eNOS pathway [50]. The cluster-1 (cytokine signaling loop) exhibited strong network interaction with cluster-2 (growth factor signaling loop), which is also correlated with cluster-3 (angiogenic signaling loop). These results indicate that D-pEMF treatment induced the paracrine signaling of hBMSCs towards osteogenesis and angiogenesis. Scheme 2 depicts an overview of the altered signaling and cell behavior upon D-pEMF on hBMSCs regulating hBMSCs proliferation and osteogenic differentiation.

4. Discussion

An alternate strategy that has recently gained attraction is called bone tissue engineering (BTE), which uses an external scaffold to supply regulatory growth hormones that stimulate cell proliferation. These implanted scaffolds must have the same osteoinductivity, osteoconductivity, biocompatibility, and appropriate mechanical strength as the original tissues [51–56]. For bone tissue remodeling, a variety of synthetic implantable scaffolds are produced, such as metal, biopolymer, bio ceramic, and composite implants [57–60]. Bone regeneration is very promising, but there are still deadly issues with bone tissue regeneration. These include growth factor carcinogenicity, high cost, and failure to form a natural combination with surrounding normal tissue [61].

Furthermore, problems with osteolysis, inflammation, and loosening of implants still need to be resolved. In addition, mechanical stimuli like stress, strain, fluid movement, electromagnetic field, and forces produced by cellular interactions are continuously applied to cells. MSCs' ability to perceive mechanical inputs from the outside world and then transmit signals downstream controls the formation and development of bones [62]. A wide range of bioreactor platforms, which speed up bone regeneration, have been developed. These systems include ultrasound bioreactors, compression bioreactors, load-bearing fluid flow shear stress-based bioreactors, tension bioreactors, multimodal bioreactors, and compression bioreactors [63].

In this study, we have studied the impact of pEMF stimuli under dynamic conditions to induce osteogenesis. Based on the conventional existing methods of bone regeneration, such as the development of scaffolds and using bandages, offer certain complications, including degradation complexity and inflammation. Herein, we have developed a multiple stimuli-responsive bioreactor system that offers a number of benefits, such as promoting cell proliferation, osteo-commitment, and production of bioactive molecules, which gives a non-invasive

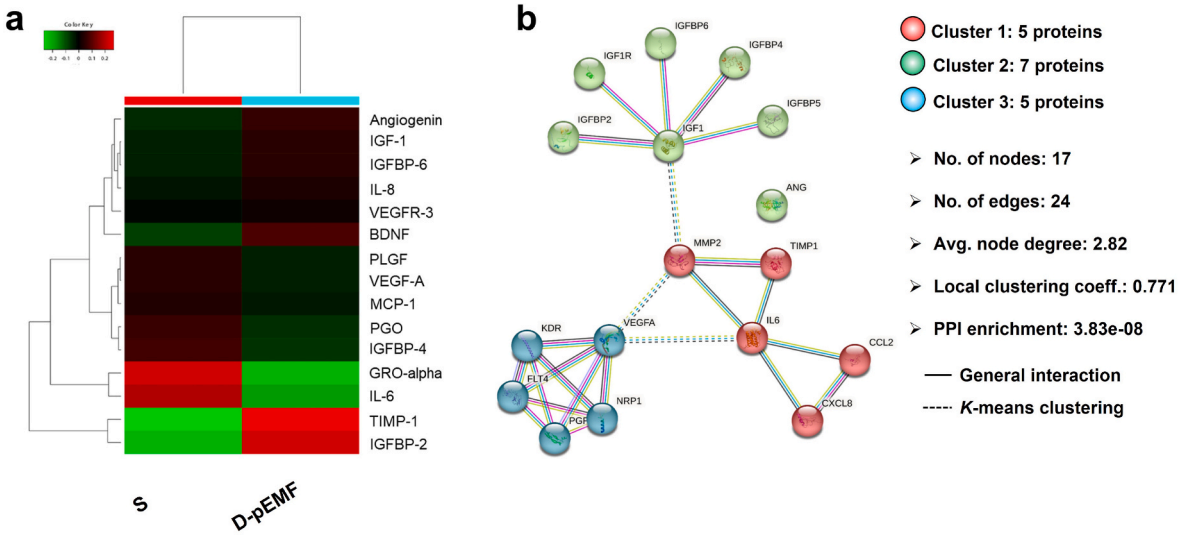

Fig. 8. Secretome analysis of the hBMSCs under S and D-pEMF conditions. Representative **(a)** Heatmap showing the expression of some selected proteins either up- or down-regulated during osteo-induction in D-pEMF and S culture. **(b)** STRING protein-protein interaction study of the identified proteins from the growth factor and cytokine arrays.

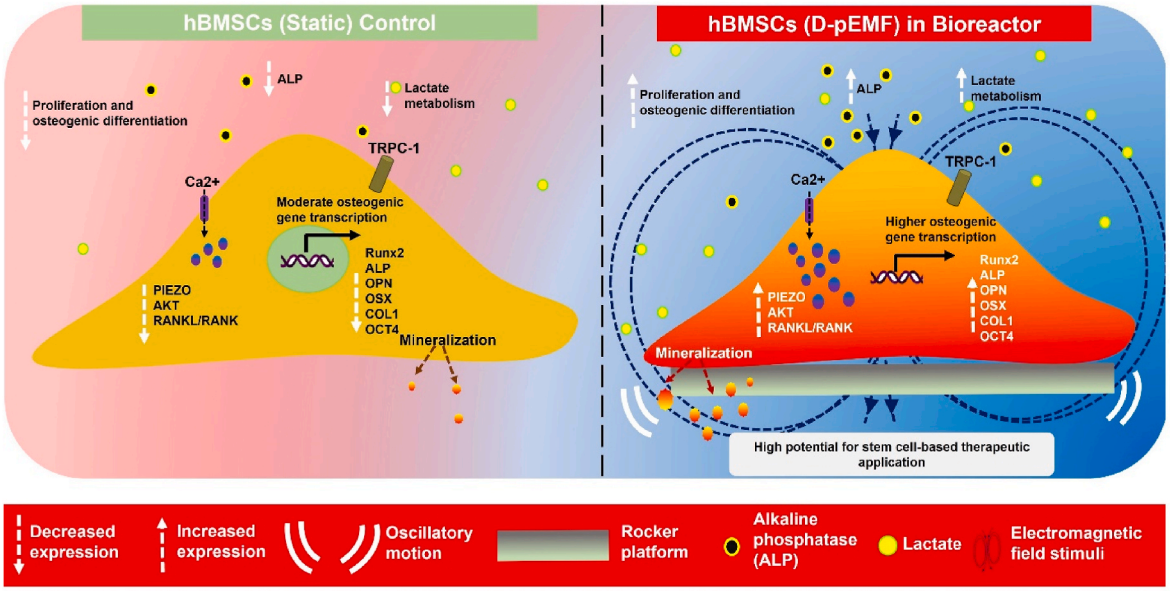

Scheme 2. Schematic overview of the study. Regulation of signaling pathways and changes under the wave motion bioreactor system-based D-pEMF stimuli.

therapeutic approach to crossing the barriers associated with existing methods. Additionally, the reactive oxygen species (ROS) or free radical system plays an important role in osteogenesis. The higher production of these leads to cellular damage and inhibits osteogenesis. Our results revealed that upon exposure of cells to D-pEMF stimuli, the cells exhibit higher levels of ROS scavenging properties. These finding indicates the potential of a multi-stimulated bioreactor system in promoting anti-oxidative properties required for healthy bone tissue development.

The gene expression study (qRT-PCR) and the transcriptomic study revealed the involvement of many signaling pathways that assist the osteogenic commitment. For instance, the Smad are proteins that function as signal transducers in transforming growth factor beta TGF-β superfamily, including bone morphogenetic proteins, activins, and Smads. The TGF-β signaling pathway regulates cellular differentiation, apoptosis, proliferation, and migration. In TGF-β signaling, the BMP ligand binds to its corresponding receptor BMPR1 and results in phosphorylation of Smad1/5/8, which in turn forms a complex with co-Smad (Smad4). The translocation of this heterotrimeric complex in the nucleus allows the transcription of various osteoblast differentiation and neurogenesis-specific genes. The mitogen-activated protein kinase (MAPKs), a family of serine/threonine kinases that responds to multiple stimuli, plays a significant role in bone development and are the primary transducers in regulating bone mass [64,65] Jun amino-terminal kinases (JNK)-1/2/3 extracellular signal-related kinases (ERKs)-1/2, p38 proteins (α/β/ϒ/δ) and ERK-5, are four differently regulated classes of MAPKs. In early osteogenic differentiation, the mixed lineage kinase (MLK3) (member of MAPK3 family) activates the MAP2Ks (MEK1/2), which in turn phosphorylates the ERK-1 and ERK-2 and results in transcription of osteogenic-specific genes such as Runx2 [41]. Hippo and Wnt signaling pathways are another essential signaling capable of inducing osteogenic differentiation [66,67]. The Hippo and Wnt signaling pathways cooperate to regulate several biological cycles. The binding of Wnt to its receptor Frizzled (FZD) allows the interaction of AXIN to the phosphorylated lipoprotein receptor-related protein (LRP), which then releases the β-catenin from the destruction complex [68]. β-catenin then interacts with Yes-associated protein-1/Transcription adaptor putative zinc finger (YAP/TAZ) and induces osteogenesis-promoting gene transcription [67,69]. Depending on the data we obtained, our research confirmed that the D-pEMF stimulation causes transcriptomic alterations in the hBMSCs. The transcriptomic alterations result from the stimulation of different signaling pathways, which leads the cells toward osteogenic commitment. Our findings revealed an increase in the osteogenesis potential of cells cultured under D-pEMF conditions. Various parameters, such as mineralization study, gene expression, and protein expression analysis, revealed the potential of hBMSCs to promote osteogenesis in an osteogenic medium. However, the D-pEMF-treated group surpasses the osteogenic potential of the cells cultured in osteogenic culture media under static conditions. A number of factors contributed to the effectiveness of D-pEMF-induced higher osteogenic differentiation over static culture under an osteogenic medium. We discovered that the D-pEMF stimulated cells allow various alterations in a number of physiological conditions, such as differential expression of genes relevant to osteogenesis, proliferation, and mineralization, which in turn causes the osteogenic differentiation of the cells. In our study, we have examined the D-pEMF stimulation of the hBMSCs grown in osteogenic media, which substantially enhanced the osteogenic potential of the cells. Yet, it is noteworthy that the hBMSCs cultured in an osteogenic medium without any stimuli exhibited low or basal-level osteogenic and ROS scavenging characteristics compared to the D-pEMF stimuli-treated groups. To elucidate this remarkable occurrence, we must comprehend the process via which EMF influences BMSCs. A crucial element of bone development is largely regulated by TGF-β and BMP signaling pathways [70]. They control the differentiation of BMSCs by interacting with the tetrameric receptor complex and initiating a downstream cascade response [71]. The BMP ligand is a member of the TGF-β family and binds to BMP receptors, namely, type I and type II, present on the cell membrane. Following the ligand and receptor binding, the type I and type II receptor homodimer combine and result in the formation of a tetramer complex, which causes the type I receptor to become *trans*-phosphorylated. Following the influence of Smad4, the phosphorylated receptor (type I) attaches to the Smad1/5/8 and reaches the nucleus, after which these proteins assemble Runx2 and several cofactors to control the osteogenic gene expression [71,72]. Subsequent studies confirmed that EMF can stimulate the gene expression level of BMPR1A, BMPR1B, BMPR2, Smad4, and Smad1/5/8. The presence of an inhibitor of the BMP type I receptor reduced the EMF-mediated regulation of BMSCs. These findings support that EMF-mediated BMPsignaling plays an essential role in osteogenic differentiation [73–75]. Therefore, from the obtained results, we can postulate that hBMSCs cultured in osteogenic medium under static conditions exhibited a lower gene expression of Smad 1 and TGF-β, which indicates that these signaling pathways were not fully activated in

the S group. Meanwhile, the D-pEMF group showed an increased gene expression of Smad 1 and TGF-β, indicating the role of D-pEMF in the activation of signaling pathways, which promotes higher osteogenesis in the treated group. Thus, combining wave motion stimuli with pEMF leads to synergistic effects on hBMSC differentiation and cell behavior.

Nevertheless, additional research studies with extended follow-up are required to confirm the efficacy of D-pEMF in treating bone-related diseases. However, with the increasing clinical demand and therapeutic application, expanding MSCs is considered a "sacred grail" for the healthcare sector. The *in vitro* expansion of MSCs by culturing them in a bioreactor system helps overcome the issues associated with the clinical challenges. The pEMF exposure is a physical therapy with several advantageous effects on bone diseases. Studies have reported that the pEMF influences the adenosine receptors, calcium channels, Wnt1, BMP2, mTOR, Notch, MAPK, and eNOS for osteoblasts. Significant therapies available for musculoskeletal disease include physical therapy, drugs, and surgery. Developing therapies based on physical stimuli is more efficient, less expensive, and non-invasive than drugs and surgeries [76]. The ambitious aim for bone-related disease is the large-scale production of MSCs, osteogenic commitment, and efficient biologically derived active molecules enabling both cell-based and cell-free therapies. To the best of our knowledge, our research successfully revealed the positive effect of pEMF on MSCs cultured in a bioreactor system. We further looked into the underlying process and discovered that the biological consequences of the pEMF influencing cell proliferation and differentiation were transmitted by the different signaling pathways [40,77].

5. Conclusion

Recent research reveals that pEMF is typically safe and can cause a variety of apparent actions in cultured bone cells. However, the mechanism still needs to be better comprehended, and optimization is needed depending on the cell type, disease stage, developmental stage, tissue microenvironment, and pEMF parameters. The main aim of this research was to outline the essential procedural conditions for the large-scale production of hBMSCs in a wave motion bioreactor system using pEMF stimulation.

For this aim, hBMSCs were examined under different pEMF exposures (1V, 5V, and 10V-1Hz, 5.82 G) to determine the optimum viability for cell expansion. In our previous study, we explored the implications of pEMFs on the cellular and molecular changes of hBMSCs [78]. Interestingly, the cells cultured in the rocking environment with an influence of 10V-1Hz pEMF under dynamic motion (35 oscillations per minute) and a magnetic field of 5.82 G exhibited improved cell viability hBMSCs >15 % than the static culture and displayed morphologies varying from spindle to globular shape following 2 weeks of culture. The cell-derived small molecules promote osteogenesis by improving the alkaline phosphatase and calcium activity. Additionally, the prolonged culture of hBMSCs in a wave-motion bioreactor dramatically boosted the expression level of osteogenesis-related gene markers. The alizarin Red-S (ARS) and alkaline phosphatase (ALP) staining results further disclose the osteogenic potential of the D-pEMF treatment as a promising culture condition for hBMSCs. The RNA-sequencing (RNA-Seq) outcomes more thoroughly show the upregulation of several key osteogenic and mechanically triggered signaling pathways during wave-motion culture.

The data obtained in this study dictate that a pEMF and dynamic motion mimic the cell microenvironment, resulting in increased metabolism and proven effective for developing tissue regenerative therapies. The bioreactor-based system provides a robust platform for understanding the pEMF-induced cell growth and development mechanism. Consequently, this study makes substantial progress in the perspective of the use of D-pEMF and its potential in tissue regeneration. This research is promising for stem cell-based therapeutic application through the use of preconditioned hBMSC transplantation, as well as the secretome, which has the potential to become a powerful tool in regenerative medicine and numerous therapeutic applications.

CRediT authorship contribution statement

Aayushi Randhawa: Writing – review & editing, Writing – original draft, Visualization, Validation, Methodology, Investigation, Formal analysis, Data curation, Conceptualization. **Keya Ganguly:** Writing – review & editing, Writing – original draft, Visualization, Validation, Supervision, Investigation, Formal analysis, Data curation. **Sayan Deb Dutta:** Writing – review & editing, Writing – original draft, Methodology, Investigation, Formal analysis, Data curation. **Tejal V. Patil:** Writing – review & editing, Visualization. **Ki-Taek Lim:** Supervision, Funding acquisition, Formal analysis.

Declaration of competing interest

The authors declare that they have no known competing financial interests or personal relationships that could have appeared to influence the work reported in this paper.

Data availability

Data will be made available on request.

Acknowledgments

This study was supported by the "Basic Science Research Program" through the "National Research Foundation of Korea" funded by the "Ministry of Education" (NRF2022R1I1A3063302 and NRF2018R1A6A1A03025582) and the Starting Growth Technological R&D program (S2840309, Biomechagen Co., Ltd.) funded by the Small and Medium Business Administration (SMBA). This work was also supported by Innovative Human Resource Development for Local Intellectualization program through the Institute of Information & Communications Technology Planning & Evaluation (IITP) grant funded by the Korea government (MSIT) (IITP-2024-RS-2023-00260267).

Appendix A. Supplementary data

Supplementary data to this article can be found online at https://doi.org/10.1016/j.biomaterials.2024.122713.

References

[1] A. Brydone, D. Meek, S. Maclaine, Bone grafting, orthopaedic biomaterials, and the clinical need for bone engineering, Proc. IME H J. Eng. Med. 224 (12) (2010) 1329–1343.
[2] G.G. Walmsley, R.C. Ransom, E.R. Zielins, T. Leavitt, J.S. Flacco, M.S. Hu, A.S. Lee, M.T. Longaker, D.C. Wan, Stem cells in bone regeneration, Stem cell reviews and reports 12 (2016) 524–529.
[3] L.F. Adolpho, H.B. Lopes, G.P. Freitas, D. Weffort, G.G. Campos Totoli, A.C. Loyola Barbosa, R.I. Freire Assis, K.G. Silverio Ruiz, D.C. Andia, A.L. Rosa, Human periodontal ligament stem cells with distinct osteogenic potential induce bone formation in rat calvaria defects, Regen. Med. 17 (6) (2022) 341–353.
[4] A.L.G. Almeida, G.P. Freitas, H.B. Lopes, R. Gimenes, S. Siessere, L.G. Sousa, M. M. Beloti, A.L. Rosa, Effect of stem cells combined with a polymer/ceramic membrane on osteoporotic bone repair. Brazilian Oral Research 33, 2019.
[5] M.M. Beloti, L.G. Sicchieri, P.T. de Oliveira, A.L. Rosa, The influence of osteoblast differentiation stage on bone formation in autogenously implanted cell-based poly (lactide-co-glycolide) and calcium phosphate constructs, Tissue Eng. 18 (9–10) (2012) 999–1005.
[6] G.P. Freitas, H.B. Lopes, A.T. P Souza, P.G. Fp Oliveira, A.L.G. Almeida, P. G. Coelho, F.U. Ferreira, D.T. Covas, M.M. Beloti, A.L. Rosa, Effect of cell therapy with osteoblasts differentiated from bone marrow or adipose tissue stromal cells on bone repair, Regenerative medicine 14 (12) (2019) 1107–1119.
[7] A.S. Mao, D.J. Mooney, Regenerative medicine: current therapies and future directions, Proc. Natl. Acad. Sci. USA 112 (47) (2015) 14452–14459.
[8] M.S. Hossain, D. Bergstrom, X. Chen, Modelling and simulation of the chondrocyte cell growth, glucose consumption and lactate production within a porous tissue scaffold inside a perfusion bioreactor, Biotechnology Reports 5 (2015) 55–62.
[9] T.R. Heathman, A.W. Nienow, Q.A. Rafiq, K. Coopman, B. Kara, C.J. Hewitt, Agitation and aeration of stirred-bioreactors for the microcarrier culture of human

mesenchymal stem cells and potential implications for large-scale bioprocess development, Biochem. Eng. J. 136 (2018) 9–17.
[10] C. Kropp, D. Massai, R. Zweigerdt, Progress and challenges in large-scale expansion of human pluripotent stem cells, Process Biochemistry 59 (2017) 244–254.
[11] L.V.G. Gil, H. Singh, J.d.S. da Silva, D.P. dos Santos, D.T. Covas, K. Swiech, C.A. T. Suazo, Feasibility of the taylor vortex flow bioreactor for mesenchymal stromal cell expansion on microcarriers, Biochem. Eng. J. 162 (2020) 107710.
[12] P. Liu, J. Tu, W. Wang, Z. Li, Y. Li, X. Yu, Z. Zhang, Effects of mechanical stress stimulation on function and expression mechanism of osteoblasts, Front. Bioeng. Biotechnol. 10 (2022) 830722.
[13] J.C. Silva, P. Marcelino, J. Meneses, F. Barbosa, C.S. Moura, A.C. Marques, J. M. Cabral, P. Pascoal-Faria, N. Alves, J. Morgado, Synergy between 3D-extruded electroconductive scaffolds and electrical stimulation to improve bone tissue engineering strategies, J. Mater. Chem. B 12 (11) (2024) 2771–2794.
[14] A.T. Semeano, F.A. Tofoli, J.C. Correa-Velloso, A.P. de Jesus Santos, A. Oliveira-Giacomelli, R.R. Cardoso, M.A. Pessoa, E.L. da Rocha, G. Ribeiro, M.F. Ferrari, Effects of magnetite nanoparticles and static magnetic field on neural differentiation of pluripotent stem cells, Stem Cell Reviews and Reports 18 (4) (2022) 1337–1354.
[15] P. Jiang, Y. Zhang, C. Zhu, W. Zhang, Z. Mao, C. Gao, Fe3O4/BSA particles induce osteogenic differentiation of mesenchymal stem cells under static magnetic field, Acta Biomater. 46 (2016) 141–150.
[16] A.S. Safavi, A. Sendera, N. Haghighipour, A. Banas-Zabczyk, The role of low-frequency electromagnetic fields on mesenchymal stem cells differentiation: a systematic review, Tissue Engineering and Regenerative Medicine 19 (6) (2022) 1147–1160.
[17] S. Weinbaum, J.M. Tarbell, E.R. Damiano, The structure and function of the endothelial glycocalyx layer, Annu. Rev. Biomed. Eng. 9 (2007) 121–167.
[18] K.F. Eichholz, I. Woods, M. Riffault, G.P. Johnson, M. Corrigan, M.C. Lowry, N. Shen, M.-N. Labour, K. Wynne, L. O'Driscoll, D.A. Hoey, Human bone marrow stem/stromal cell osteogenesis is regulated via mechanically activated osteocyte-derived extracellular vesicles, Stem Cells Translational Medicine 9 (11) (2020) 1431–1447.
[19] T. Yi, S. Huang, G. Liu, T. Li, Y. Kang, Y. Luo, J. Wu, Bioreactor synergy with 3D scaffolds: new era for stem cells culture, ACS Appl. Bio Mater. 1 (2) (2018) 193–209.
[20] J.S. Khaw, R. Xue, N.J. Cassidy, S.H. Cartmell, Electrical stimulation of titanium to promote stem cell orientation, elongation and osteogenesis, Acta Biomater. 139 (2022) 204–217.
[21] J.d.S. da Silva, A. Mizukami, L.V.G. Gil, J.V. de Campos, O.B. Assis, D.T. Covas, K. Swiech, C.A.T. Suazo, Improving wave-induced motion bioreactor performance for human mesenchymal stromal cell expansion, Process biochemistry 84 (2019) 143–152.
[22] K. Ganguly, S.D. Dutta, A. Randhawa, D.K. Patel, T.V. Patil, K.T. Lim, Transcriptomic changes toward osteogenic differentiation of mesenchymal stem cells on 3D-printed GelMA/CNC hydrogel under pulsatile pressure environment, Adv. Healthcare Mater. 12 (11) (2023) 2202163.
[23] H. Shi, K. Zhou, M. Wang, N. Wang, Y. Song, W. Xiong, S. Guo, Z. Yi, Q. Wang, S. Yang, Integrating physicomechanical and biological strategies for BTE: biomaterials-induced osteogenic differentiation of MSCs, Theranostics 13 (10) (2023) 3245.
[24] S.D. Dutta, J. Bin, K. Ganguly, D.K. Patel, K.-T. Lim, Electromagnetic field-assisted cell-laden 3D printed poloxamer-407 hydrogel for enhanced osteogenesis, RSC Adv. 11 (33) (2021) 20342–20354.
[25] S.D. Dutta, D.K. Patel, Y.-R. Seo, C.-W. Park, S.-H. Lee, J.-W. Kim, J. Kim, H. Seonwoo, K.-T. Lim, In vitro biocompatibility of electrospun poly (ε-Caprolactone)/Cellulose nanocrystals-nanofibers for tissue engineering, J. Nanomater. 2019 (2019).
[26] M. Samiei, Z. Aghazadeh, E.D. Abdolahinia, A. Vahdati, S. Daneshvar, A. Noghani, The effect of electromagnetic fields on survival and proliferation rate of dental pulp stem cells, Acta Odontol. Scand. 78 (7) (2020) 494–500.
[27] M. Zhang, X. Li, L. Bai, K. Uchida, W. Bai, B. Wu, W. Xu, H. Zhu, H. Huang, Effects of low frequency electromagnetic field on proliferation of human epidermal stem cells: an in vitro study, Bioelectromagnetics 34 (1) (2013) 74–80.
[28] V. Zablotskii, T. Polyakova, O. Lunov, A. Dejneka, How a high-gradient magnetic field could affect cell life Sci, Rep 6 (2016) 37407.
[29] K. Song, S.H. Im, Y.J. Yoon, H.M. Kim, H.J. Lee, G.S. Park, A 60 Hz uniform electromagnetic field promotes human cell proliferation by decreasing intracellular reactive oxygen species levels, PLoS One 13 (7) (2018) e0199753.
[30] C. Osera, M. Amadio, S. Falone, L. Fassina, G. Magenes, F. Amicarelli, G. Ricevuti, S. Govoni, A. Pascale, Pre-exposure of neuroblastoma cell line to pulsed electromagnetic field prevents H2O2-induced ROS production by increasing MnSOD activity, Bioelectromagnetics 36 (3) (2015) 219–232.
[31] R. Brigelius-Flohé, A.P. Kipp, Physiological functions of GPx2 and its role in inflammation-triggered carcinogenesis, Ann. N. Y. Acad. Sci. 1259 (1) (2012) 19–25.
[32] F. Chen, Y. Liu, N.-K. Wong, J. Xiao, K.-F. So, Oxidative stress in stem cell aging, Cell Transplant. 26 (9) (2017) 1483–1495.
[33] A. Campisi, M. Gulino, R. Acquaviva, P. Bellia, G. Raciti, R. Grasso, F. Musumeci, A. Vanella, A. Triglia, Reactive oxygen species levels and DNA fragmentation on astrocytes in primary culture after acute exposure to low intensity microwave electromagnetic field, Neurosci. Lett. 473 (1) (2010) 52–55.
[34] L. Wang, X. You, L. Zhang, C. Zhang, W. Zou, Mechanical regulation of bone remodeling, Bone Research 10 (1) (2022) 16.
[35] X. Wang, Y. Yang, Y. Wang, C. Lu, X. Hu, N. Kawazoe, Y. Yang, G. Chen, Focal adhesion and actin orientation regulated by cellular geometry determine stem cell differentiation via mechanotransduction, Acta Biomaterialia 182 (2024) 81–92.
[36] J. Pablo Rodríguez, M. González, S. Ríos, V. Cambiazo, Cytoskeletal organization of human mesenchymal stem cells (MSC) changes during their osteogenic differentiation, J. Cell. Biochem. 93 (4) (2004) 721–731.
[37] X. Zhang, T. Wang, Z. Zhang, H. Liu, L. Li, A. Wang, J. Ouyang, T. Xie, L. Zhang, J. Xue, Electrical stimulation system based on electroactive biomaterials for bone tissue engineering, Mater. Today (2023).
[38] Z. Chen, J. Zheng, X. Pei, S. Sun, J. Cai, Y. Liu, Y. Wang, L. Zheng, H. Zhou, Ultrasound-driven electrical stimulation based on 3D hierarchical porous piezoelectric nanofiber-aerogel scaffold promotes bone defect repair, Chem. Eng. J. (2023) 144305.
[39] K.H. Dittmann, C. Mayer, H. Stephan, C. Mieth, M. Bonin, B. Lechmann, H. P. Rodemann, Exposure of primary osteoblasts to combined magnetic and electric fields induced spatiotemporal endochondral ossification characteristic gene-and protein expression profiles, Journal of Experimental Orthopaedics 9 (1) (2022) 1–14.
[40] J. Yan, C. Liu, C. Tu, R. Zhang, X. Tang, H. Li, H. Wang, Y. Ma, Y. Zhang, H. Wu, Hydrogel-hydroxyapatite-monomeric collagen type-I scaffold with low-frequency electromagnetic field treatment enhances osteochondral repair in rabbits, Stem Cell Res. Ther. 12 (1) (2021) 1–21.
[41] G. Choe, M. Lee, S. Oh, J.M. Seok, J. Kim, S. Im, S.A. Park, J.Y. Lee, Three-dimensional bioprinting of mesenchymal stem cells using an osteoinductive bioink containing alginate and BMP-2-loaded PLGA nanoparticles for bone tissue engineering, Biomaterials advances 136 (2022) 212789.
[42] W. Sun, S. Chi, Y. Li, S. Ling, Y. Tan, Y. Xu, F. Jiang, J. Li, C. Liu, G. Zhong, D. Cao, X. Jin, D. Zhao, X. Gao, Z. Liu, B. Xiao, Y. Li, The mechanosensitive Piezo1 channel is required for bone formation, Elife 8 (2019).
[43] L. Ma, R. Aijima, Y. Hoshino, H. Yamaza, E. Tomoda, Y. Tanaka, S. Sonoda, G. Song, W. Zhao, K. Nonaka, Transplantation of mesenchymal stem cells ameliorates secondary osteoporosis through interleukin-17-impaired functions of recipient bone marrow mesenchymal stem cells in MRL/lpr mice, Stem Cell Res. Ther. 6 (2015) 1–17.
[44] N. Baker, J. Sohn, R.S. Tuan, Promotion of human mesenchymal stem cell osteogenesis by PI3-kinase/Akt signaling, and the influence of caveolin-1/cholesterol homeostasis, Stem Cell Res. Ther. 6 (1) (2015) 1–11.
[45] M. Beederman, J.D. Lamplot, G. Nan, J. Wang, X. Liu, L. Yin, R. Li, W. Shui, H. Zhang, S.H. Kim, W. Zhang, J. Zhang, Y. Kong, S. Denduluri, M.R. Rogers, A. Pratt, R.C. Haydon, H.H. Luu, J. Angeles, L.L. Shi, T.C. He, BMP signaling in mesenchymal stem cell differentiation and bone formation, J. Biomed. Sci. Eng. 6 (8a) (2013) 32–52.
[46] Q. Liu, L. Lei, T. Yu, T. Jiang, Y. Kang, Effect of brain-derived neurotrophic factor on the neurogenesis and osteogenesis in bone engineering, Tissue Eng. 24 (15–16) (2018) 1283–1292.
[47] T. Liang, W. Gao, L. Zhu, J. Ren, H. Yao, K. Wang, D. Shi, TIMP-1 inhibits proliferation and osteogenic differentiation of hBMSCs through Wnt/β-catenin signaling, Biosci. Rep. 39 (1) (2019) BSR20181290.
[48] D. Fan, H. Liu, Z. Zhang, M. Su, Z. Yuan, Y. Lin, S. Yang, W. Li, X. Zhang, Resveratrol and angiogenin-2 combined with PEGDA/TCS hydrogel for the targeted therapy of hypoxic bone defects via activation of the autophagy pathway, Front. Pharmacol. 12 (2021) 618724.
[49] G. Xi, C. Wai, V. DeMambro, C.J. Rosen, D.R. Clemmons, IGFBP-2 directly stimulates osteoblast differentiation, J. Bone Miner. Res. 29 (11) (2014) 2427–2438.
[50] C.-N. Hao, J.-J. Huang, Y.-Q. Shi, X.-W. Cheng, H.-Y. Li, L. Zhou, X.-G. Guo, R.-L. Li, W. Lu, Y.-Z. Zhu, Pulsed electromagnetic field improves cardiac function in response to myocardial infarction, American journal of translational research 6 (3) (2014) 281.
[51] G. Turnbull, J. Clarke, F. Picard, P. Riches, L. Jia, F. Han, B. Li, W. Shu, 3D bioactive composite scaffolds for bone tissue engineering, Bioact. Mater. 3 (3) (2018) 278–314.
[52] L. Leppik, H. Zhihua, S. Mobini, V. Thottakkattumana Parameswaran, M. Eischen-Loges, A. Slavici, J. Helbing, L. Pindur, K.M. Oliveira, M.B. Bhavsar, Combining electrical stimulation and tissue engineering to treat large bone defects in a rat model, Sci. Rep. 8 (1) (2018) 6307.
[53] R. Eivazzadeh-Keihan, E. Bahojb Noruzi, K. Khanmohammadi Chenab, A. Jafari, F. Radinekiyan, S.M. Hashemi, F. Ahmadpour, A. Behboudi, J. Mosafer, A. Mokhtarzadeh, Metal-based nanoparticles for bone tissue engineering, Journal of Tissue Engineering and Regenerative Medicine 14 (12) (2020) 1687–1714.
[54] M.P. Nikolova, M.S. Chavali, Recent advances in biomaterials for 3D scaffolds: a review, Bioact. Mater. 4 (2019) 271–292.
[55] M.M. Islam, M. Shahruzzaman, S. Biswas, M.N. Sakib, T.U. Rashid, Chitosan based bioactive materials in tissue engineering applications-A review, Bioact. Mater. 5 (1) (2020) 164–183.
[56] C. Wang, W. Huang, Y. Zhou, L. He, Z. He, Z. Chen, X. He, S. Tian, J. Liao, B. Lu, 3D printing of bone tissue engineering scaffolds, Bioact. Mater. 5 (1) (2020) 82–91.
[57] F. Shang, Y. Yu, S. Liu, L. Ming, Y. Zhang, Z. Zhou, J. Zhao, Y. Jin, Advancing application of mesenchymal stem cell-based bone tissue regeneration, Bioact. Mater. 6 (3) (2021) 666–683.
[58] J.M. Sadowska, M.-P. Ginebra, Inflammation and biomaterials: role of the immune response in bone regeneration by inorganic scaffolds, J. Mater. Chem. B 8 (41) (2020) 9404–9427.
[59] K. Lin, L. Xia, H. Li, X. Jiang, H. Pan, Y. Xu, W.W. Lu, Z. Zhang, J. Chang, Enhanced osteoporotic bone regeneration by strontium-substituted calcium silicate bioactive ceramics, Biomaterials 34 (38) (2013) 10028–10042.

[60] C. Wang, B. Chen, W. Wang, X. Zhang, T. Hu, Y. He, K. Lin, X. Liu, Strontium released bi-lineage scaffolds with immunomodulatory properties induce a pro-regenerative environment for osteochondral regeneration, Mater. Sci. Eng. C 103 (2019) 109833.
[61] A.C. Marsh, N.P. Mellott, N. Pajares-Chamorro, M. Crimp, A. Wren, N.D. Hammer, X. Chatzistavrou, Fabrication and multiscale characterization of 3D silver containing bioactive glass-ceramic scaffolds, Bioact. Mater. 4 (2019) 215–223.
[62] Y. Sun, B. Wan, R. Wang, B. Zhang, P. Luo, D. Wang, J.-J. Nie, D. Chen, X. Wu, Mechanical stimulation on mesenchymal stem cells and surrounding microenvironments in bone regeneration: regulations and applications, Front. Cell Dev. Biol. 10 (2022) 808303, 808303.
[63] F.M. Shaikh, T.P. O'Brien, A. Callanan, E.G. Kavanagh, P.E. Burke, P.A. Grace, T. M. McGloughlin, New pulsatile hydrostatic pressure bioreactor for vascular tissue-engineered constructs, Artif. Organs 34 (2) (2010) 153–158.
[64] C. Ge, G. Xiao, D. Jiang, R.T. Franceschi, Critical role of the extracellular signal–regulated kinase–MAPK pathway in osteoblast differentiation and skeletal development, The Journal of cell biology 176 (5) (2007) 709–718.
[65] C. Ge, G. Xiao, D. Jiang, Q. Yang, N.E. Hatch, H. Roca, R.T. Franceschi, Identification and functional characterization of ERK/MAPK phosphorylation sites in the Runx2 transcription factor, J. Biol. Chem. 284 (47) (2009) 32533–32543.
[66] W.P. Cawthorn, A.J. Bree, Y. Yao, B. Du, N. Hemati, G. Martinez-Santibañez, O. A. MacDougald, Wnt6, Wnt10a and Wnt10b inhibit adipogenesis and stimulate osteoblastogenesis through a β-catenin-dependent mechanism, Bone 50 (2) (2012) 477–489.
[67] R. Vlashi, X. Zhang, M. Wu, G. Chen, Wnt signaling: essential roles in osteoblast differentiation, bone metabolism and therapeutic implications for bone and skeletal disorders, Genes & Diseases 10 (4) (2023) 1291–1317.
[68] J. Liu, Q. Xiao, J. Xiao, C. Niu, Y. Li, X. Zhang, Z. Zhou, G. Shu, G. Yin, Wnt/β-catenin signalling: function, biological mechanisms, and therapeutic opportunities, Signal Transduct. Targeted Ther. 7 (1) (2022) 3.
[69] X. Varelas, B.W. Miller, R. Sopko, S. Song, A. Gregorieff, F.A. Fellouse, R. Sakuma, T. Pawson, W. Hunziker, H. McNeill, The Hippo pathway regulates Wnt/β-catenin signaling, Dev. Cell 18 (4) (2010) 579–591.
[70] K. Luo, Signaling cross talk between TGF-β/Smad and other signaling pathways, Cold Spring Harbor Perspect. Biol. 9 (1) (2017) a022137.
[71] M. Wu, G. Chen, Y.-P. Li, TGF-β and BMP signaling in osteoblast, skeletal development, and bone formation, homeostasis and disease, Bone Research 4 (1) (2016) 16009.
[72] G. Chen, C. Deng, Y.-P. Li, TGF-β and BMP signaling in osteoblast differentiation and bone formation, Int. J. Biol. Sci. 8 (2) (2012) 272.
[73] W. Li, W. Liu, W. Wang, J. Wang, T. Ma, J. Chen, H. Wu, C. Liu, Sinusoidal electromagnetic fields accelerate bone regeneration by boosting the multifunctionality of bone marrow mesenchymal stem cells, Stem Cell Res. Ther. 12 (2021) 1–17.
[74] C.L. Ross, M. Siriwardane, G. Almeida-Porada, C.D. Porada, P. Brink, G.J. Christ, B. S. Harrison, The effect of low-frequency electromagnetic field on human bone marrow stem/progenitor cell differentiation, Stem Cell Res. 15 (1) (2015) 96–108.
[75] C. Tu, Y. Xiao, Y. Ma, H. Wu, M. Song, The legacy effects of electromagnetic fields on bone marrow mesenchymal stem cell self-renewal and multiple differentiation potential, Stem Cell Res. Ther. 9 (2018) 1–11.
[76] B. Zhang, Y. Xie, Z. Ni, L. Chen, Effects and mechanisms of exogenous electromagnetic field on bone cells: a review, Bioelectromagnetics 41 (4) (2020) 263–278.
[77] A. Catalano, S. Loddo, F. Bellone, C. Pecora, A. Lasco, N. Morabito, Pulsed electromagnetic fields modulate bone metabolism via RANKL/OPG and Wnt/β-catenin pathways in women with postmenopausal osteoporosis: a pilot study, Bone 116 (2018) 42–46.
[78] S.D. Dutta, T. Park, K. Ganguly, D.K. Patel, J. Bin, M.-C. Kim, K.-T. Lim, Evaluation of the sensing potential of stem cell-secreted proteins via a microchip device under electromagnetic field stimulation, ACS Appl. Bio Mater. 4 (9) (2021) 6853–6864.